EURAMET

FINAL PUBLISHABLE REPORT

Grant Agreement number	15HLT01
Project short name	MetVBadBugs
Project full title	Quantitative measurement and imaging of drug uptake by bacteria with antimicrobial resistance

Project start date and duration:	01 May 2016 – 36 Months
Coordinator: Dr Paulina Rakowska, NPL, Tel: +44 208 943 7111 E-mail: paulina.rakowska@npl.co.uk Project website address: http://empir.npl.co.uk/metvbadbugs/	

Internal Funded Partners:	External Funded Partners:	Unfunded Partners:
1 NPL, United Kingdom 2 BAM, Germany 3 CMI, Czech, Republic 4 DoH, United Kingdom 5 INRIM, Italy 6 PTB, Germany	7 LENS, Italy 8 UNOTT, United Kingdom	9 FCI, United Kingdom 10 GSK, United Kingdom 11 ION-TOF, Germany 12 SNM, United Kingdom 13 SPECS, Germany
RMG: -		

Final Publishable Report

TABLE OF CONTENTS

1   Overview

The innate resistance of Gram-negative bacteria to antibiotics is a consequence of the combinatorial effects of two permeability barriers: the outer and inner bacterial cell membranes, their ability to efflux antibiotics out of the cell and their capacity to form antibiotic tolerant biofilms that are up to 100 times more resistant than planktonic bacterial cells. The objectives of this project were to advance the measurement capability by providing the urgently needed essential metrology to quantitatively measure and image the localisation of antibiotics and to understand the penetration and efflux processes in bacteria and biofilms. The objectives were met and the project developed and demonstrated a range of technologies and methods to study microbial samples. These include chemical and optical imaging, but also a range of signal enhancement strategies for further advancing the measurements. Several techniques were adopted for the measurement of the samples in their close to native state, including measurements in liquid, near-ambient pressure or frozen-hydrated. Well controlled model systems and quantitative approaches were developed to aid the metrology of bacterial samples.

2   Need

It is universally acknowledged that the threat of antimicrobial resistance (AMR) to the health and prosperity of Europe and the world is real. The European Union has a major initiative to fight AMR. The Joint Programming Initiative on Antimicrobial Resistance (JPIAMR) is developing a strategic research agenda and is co-ordinating European research in Horizon 2020, in the Innovative Medicines Initiative (IMI) and in the EC's ERA-NET funding scheme. For example, the New Drugs for Bad Bugs (ND4BB) programme of the IMI involves nine large pharmaceutical companies in seven ND4BB projects, with a total committed budget of more than €600 million. They identified a metrology gap that EMPIR was uniquely placed to fill. The ND4BB project TRANSLOCATE stated that *"At present, there are no reliable and general methods for measuring these [drug] penetration processes in Gram-negative bacteria and this bottleneck substantially hinders the ability of scientists to optimise antimicrobial activity in intact bacterial cells"*. Furthermore, they identified the key need to quantify and image the penetration of drugs into bacteria and to measure the efflux processes. MetVBadBugs was directly focused at these metrology challenges. There was clearly no single technique that can deliver all the measurement answers needed by scientists studying AMR and developing new antibiotics. A robust metrology framework was needed, which built on fundamental studies of the techniques as well as being combined with cross measurement platform validation including pre-normative studies. The objectives of this project were clearly aimed at addressing these needs.

3   Objectives

This project addressed the following scientific and technical objectives:

1. To develop urgently needed new metrological capabilities for:

   - the label-free 3D imaging of antibacterial agents in bacteria. This required a new 3D chemical imaging instrument with 100 times better sensitivity and a high-spatial resolution (100 nm). The instrument would have a mass resolution of >100 000 and the ability to sample from sub-micron areas, simultaneously.

   - the traceable quantification of the vertical concentration profile of antibacterial agents in bacteria and biofilms. Measurements would be performed in liquid and at near ambient pressure.

   - imaging surface macromolecules, such as porins or metal-transport proteins, to study the efflux mechanisms in Gram-negative bacteria and to give real-time quantitative measurements of drug-uptake in bacteria and biofilms. Numerical modelling and algorithms would be developed to support measurements in complex biological environments.

2. To develop well-controlled model systems to allow cross-platform measurement of penetration, accumulation and efflux of antibacterial agents in single cells, in suspended cellular aggregates, as well as in biofilm communities including binding to biofilm matrix components. The efficacy of novel antibacterial agents and efflux pump inhibitors would be investigated.

3. To develop signal enhancement strategies and advanced sample preparation methods for studying antibacterial agents in bacteria and biofilms including:

- advanced cryo preparation methods to enable 'liquid' (vitrified) water to be present in the vacuum of high-performance metrology instruments without ultrastructural reorganisation and translocation of exo/endo -genous molecules.

- novel methods to nano-sculpt bacteria for chemical imaging at 50 nm resolution.

- nano structured substrates for enhanced sensitivity.

4. To facilitate the take up of the technology and measurement infrastructure developed by the project by healthcare professionals (hospitals and health centres) and industry (pharmaceutical companies), in order to fight the threat from antimicrobial resistance to the health and prosperity of Europe.

4   Results

This section gives an account of the project's outputs delivered against each of the project's objectives.

4.1   Objective 1

4.1.1   *Chemical imaging by 3D OrbiSIMS*

To develop urgently needed new metrological capabilities for the label-free 3D imaging of antibacterial agents in bacteria. This requires a new 3D chemical imaging instrument with 100 times better sensitivity and a high-spatial resolution (100 nm). The instrument will have a mass resolution of >100 000 and the ability to sample from sub-micron areas, simultaneously.

The consortium developed a method for the analysis of frozen-hydrated samples by 3D OrbiSIMS. The high water content of microbial biofilms makes them difficult to image by SIMS instruments, operating in high vacuum conditions, without the loss of their native architecture. Therefore, instrumentation developments were carried out and a workflow was devised, which combines high pressure freezing, a cryo-transfer system and the advanced cryo 3D-orbiSIMS analysis. NPL, UNOTT, ION-TOF and DOH carried out the method development. The remaining partners contributed to the discussions, the choice of model system and the interpretation of data.

ION-TOF, with NPL, successfully designed, constructed and installed the load lock and the stage on the 3D OrbiSIMS instrument (placed at NPL), for cryogenic sample handling and measurements. Sample holders have been optimised so that they fit onto the cryogenic stage to accommodate high-pressure freezing planchettes. The cryo-sample transfer procedure was developed and it proved successful at preventing ice formation at the surface of the samples. Figure 1 illustrates the main components of the sample handling protocol.

NPL and DoH put considerable effort into assessing a chemical imaging cryoprotectant that is compatible with SIMS. Cryoprotectants are added to samples to prevent damage that could be caused by the high-pressure freezing process. A range of media were evaluated and a 150 mM solution of ammonium formate was chosen as the most compatible one. Ammonium formate does not interfere with SIMS analysis and it is commonly used to wash biological samples from salts, which otherwise have a very strong signal in the mass spectrum and can suppress other ions. It was also proven that it acted as an efficient cryoprotectant, which was evaluated by the TEM imaging of frozen-hydrated bacterial samples.

The operation of the instrument and the experimental conditions were optimised to allow the analysis of frozen-hydrated samples in temperatures below -180 ˚C, using two primary ion beams (gas cluster ion beam (GCIB): Ar clusters, and liquid metal ion gun (LMIG): Bi_3^+) and two analysers: time-of-flight (TOF) and Orbitrap and an analysis was performed consisting of imaging and depth profiling in single and dual beam modes. The analysis was done in close cooperation between NPL and UNOTT.
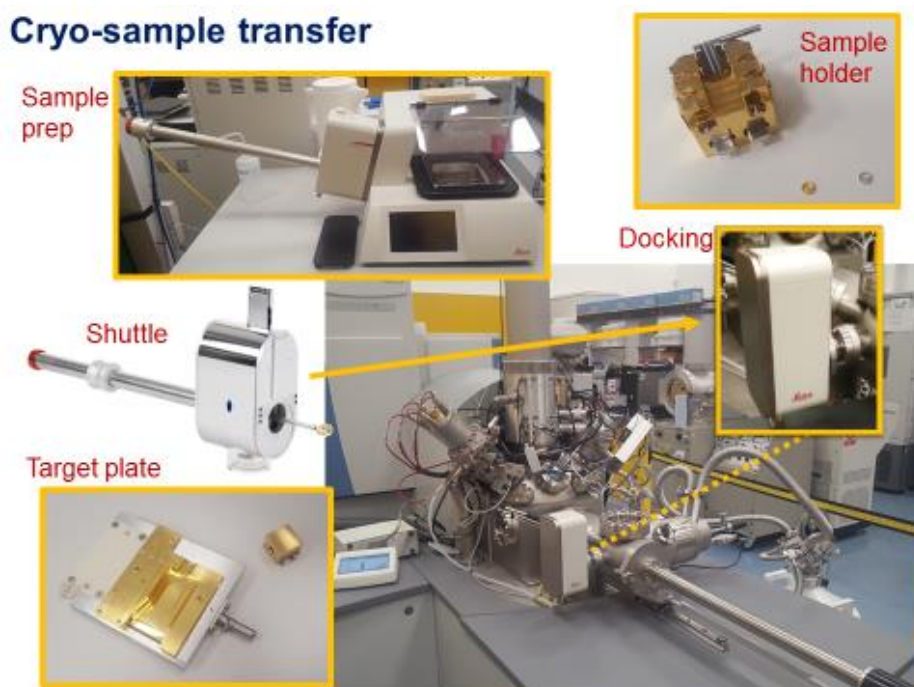
Figure 1. The cryogenic capability of the 3D-OrbiSIMS instrument to handle and measure cryogenically-prepared, by high pressure freezing, hydrated biological samples. The instrument is equipped with a vacuum cryo-transfer system, which docks a sample shuttle chamber, enabling the interchange of samples between cryo-preparative equipment and the 3D OrbiSIMS instrument in cryogenic and vacuum conditions without exposure to the ambient environment.

The method was tested on *Pseudomonas aeruginosa* biofilms. The results demonstrated the successful development of a method for the high-resolution and high-sensitivity imaging of biofilm samples. The beyond state-of-the-art aspect lies in the analysis of the samples, by secondary ion mass spectrometry, in their frozen-hydrated state. Both the instrumentation as well as the methodology were developed for sample preparation and handling and for the first time, the microbial biofilm 3D architecture was successfully probed in the close-to-native sample state. The Orbitrap analyser, in addition to the conventional ToF analyser, allows for increased method sensitivity and for mass resolving power, enabling unambiguous identification of the compounds in the samples.

The results cannot be shown in this report as they are confidential. The publication is in preparation and the data cannot be reported before manuscript submission.

Laser post ionisation was not implemented in the method. This part of the work was removed from the project.

4.1.2 *Chemical mapping of antimicrobials in small bacteria by s-SNOM*

The consortium developed and evaluated the methodology for scattering-type scanning near-field optical microscopy (s-SNOM) using mid-IR radiation for the label-free imaging of drug concentrations in particularly small bacteria. In the method described in Section 4.1.2, all of the samples were produced at DOH, who worked with UNOTT, PTB and NPL on the sample preparation protocols. PTB, with the assistance of CMI, performed analytical measurements on the samples. INRIM fabricated the optimised AFM tips. All partners contributed to the choice of the model system and in the interpretation of the data.

4.1.2.1 *Method and model system*

A commercial nano-FTIR set-up (Neaspec GmbH), adapted to synchrotron radiation at the IR-beamline of the Metrology Light Source (MLS) (P. Hermann, 2013), was used. The IR beamline provides broadband radiation, with the wavelength range of 1 µm – 20 µm being determined by the set-up and the detector, with an integrated power of 2 mW. The setup is combined with pseudoheterodyn detection and a quantum cascade laser system (Daylight Solution). The asymmetric arrangement of the interferometer incorporating the AFM tip (P. Hermann,

2013) allows both the nearfield amplitude and the phase of the radiation scattered from the AFM tip to be optimised. The relevant quantity for chemical imaging is the phase, as it matches well with the grazing-incidence FTIR spectra (S. Mastel, 2015).

The choice of model biocide was done with the input of all partners. Triclosan was chosen as the model-biocide, as it is a common antibacterial agent with a convenient IR spectrum. It works by inhibiting fatty acid synthesis. It specifically targets an enzyme called FabI (enoyl-acul carrier protein reductase). The crystal structure of the FabI-NAD$^+$-triclosan complex indicates that hydrogen bonds and hydrophobic interactions between triclosan and both the protein and the NAD$^+$ cofactor contribute to the formation of a stable ternary complex, with the drug binding at the enoyl substrate site. Triclosan is a broad-spectrum antibacterial agent that enjoys widespread applications in a multitude of contemporary consumer products including soaps, detergents, toothpastes, skin care products, cutting boards, and mattress pads. It affects bacterial membranes as fatty acid synthesis is required for their integrity. At high concentrations it will kill the bacteria (bactericidal), but at lower concentrations it will arrest growth (bacteriostatic). One of the interesting aspects is that because it shuts the cells down to a dormant phase, other antibiotics that target processes in active bacteria are no longer effective.

The calibration of the s-SNOM signal with respect to triclosan concentrations requires a material system serving as a matrix with an IR spectrum not overlapping with triclosan. In addition, a well-controlled concentration at the 10 nm scale is required. Because of the limited availability of such a calibration sample, the procedure was carried out on triclosan nanocrystals from which the sensitivity was inferred.

The *E. coli* MG1655 strain was chosen as the sample-bacterium, and it was used for s-SNOM evaluation with and without triclosan application.

4.1.2.2   Results

E. coli bacteria were treated with triclosan, washed with ammonium formate and preserved in a 'near-native' state by cryo-fixation of the sample, preserving the structure without the damaging effects of ice crystal formation or chemical fixation. The sample preparation was carried out by DOH. Then, the samples were freeze-dried. The options for freeze drying were tested by DOH, and Figure 2 shows some SEM microscopy images. Some potential collapse artefacts can be seen in some of the bacteria, as well as salt crystallisation from the buffer solution, but in general the bacterial shape was reasonably well preserved. The prepared samples were sent to PTB for analysis by s-SNOM.
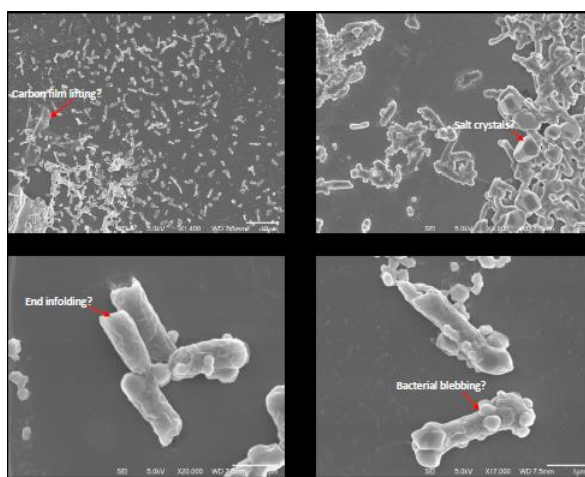

Figure 2. SEM image of the bacteria with a 4 nm platinum coat: Some evidence of freeze-drying damage on the bacterial surface are indicated, but generally the shape was good.

The sensitivity of s-SNOM for the imaging of triclosan has been evaluated by PTB, with the assistance of CMI (data not shown). In order to select the appropriate triclosan mode for its detection, Figure 3 compares the FTIR spectra of the *E. coli* sample and triclosan. The modes indicated by the dashed lines were further used to detect and quantify the triclosan in the samples. The resonance at 1600 cm^{-1} and 1474 cm^{-1} have been assigned to CC ring stretching modes with significant contributions from in-plane CH bendings, and 1100 cm^{-1} to bending of the dichloro-substituted phenoxy ring.
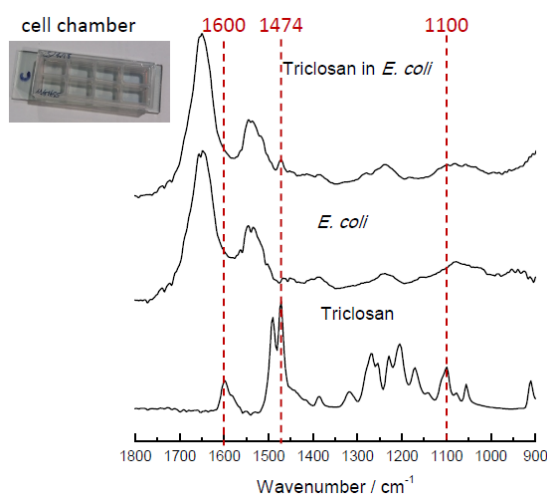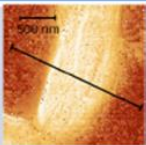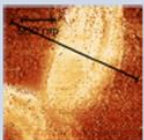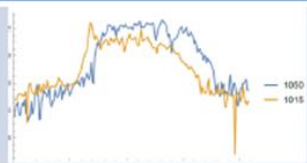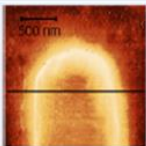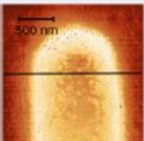
Figure 3. Comparison of the FTIR spectra of triclosan, the *E. coli* sample and the treated *E. coli* sample.

Samples treated with 2.5 % and 5 % triclosan in ethanol solution, as well as a control sample, have been imaged. A clear effect of triclosan treatment was found by imaging the individual bacteria at different wavenumbers. However, the variation could not be systematically assigned to triclosan modes. In particular, the complete quenching of the phase signal has been observed at some wavenumbers. An extreme example is shown in Table 1, which compares s-SNOM images at 1050 cm^{-1} and 1015 cm^{-1}. In the cas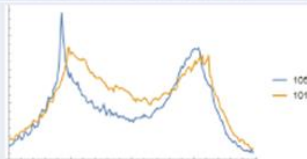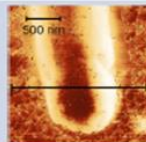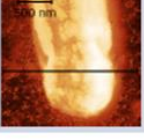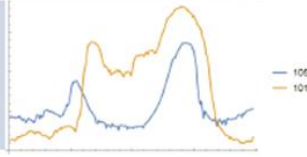e of treatment with 5 % the centres of the bacteria shows an even lower phase signal than the neighbouring gold substrate, while at 1015 cm^{-1} an internal structure becomes visible. The quenching might be an indication of a spectrally dependent probing volume: A thin but optically dense surface layer may itself not lead to a strong phase shift, but it may also prevent subsurface layers from contributing. In this case a multivariate data analysis, e.g. using cluster analysis, may result in highly complex spectral components.

Table 1. Comparison of s-SNOM images from *E. coli* treated with different concentrations of triclosan.

Triclosan conc.	1050 cm^{-1} Expect strong absorption at triclosan	1015 cm^{-1} Expect weak absorption at triclosan	Signal value (absorption) along the line
0 %			
2.5%			
5 %			

4.1.2.3   Conclusions

PTB, in cooperation with DOH, and CMI showed the potential of s-SNOM analysis to study bacteria-antibiotic interactions. Our results show a clear interaction of the drug with the bacterial membrane, suggesting that the drug accumulates between the inner and the outer membrane of the bacteria. Yet, for the results to be conclusive, further study is needed. The s-SNOM technique is very surface sensitive, i.e. it would mainly probe the top 50 nm of the sample. The bacterium is typically several hundred nanometres thick and biofilms are

typically several micrometres thick. Therefore, the measurements should be performed on 50 nm thick sections of bacteria rather than on the whole cells. This work will be continued beyond the funded period of the MetVBadBugs project.

4.1.3 *Development of XPS and XRF methods*

To develop urgently needed new metrological capabilities for the traceable quantification of the vertical concentration profile of antibacterial agents in bacteria and biofilms. Measurements will be performed in liquid and at near ambient pressure.

To address the 2nd part of objective 1 - the traceable quantification of the vertical concentration profile of antibacterial agents in bacteria and biofilms by performing measurements in liquid and at near ambient pressure - X-ray based techniques such as X-Ray Photoelectron Spectroscopy (XPS), and X-Ray Fluorescence analysis (XRF) were applied. Here, mainly BAM, SPECS and PTB were involved. They were supported e.g. in the field of sample preparation by UNOTT and NPL. The aim was to extend these already well-established measurement techniques to measure the uptake of antimicrobial agents or biocides in biofilms if possible in their natural conditions. Because of strong absorption effects these X-ray-based techniques need to be carried out at high vacuum levels of better than 10^{-6} mbar. Bacteria are inherently in a hydrated state and are therefore not compatible for use with these ultra-high vacuum techniques without prior sample preparation involving freeze drying or fast freezing. Hence, two of the main aims of the project were to establish Near-Ambient Pressure XPS (NAP-XPS) for the consortium and to evaluate its potential use in biology-related fields. NAP-XPS makes it possible to characterise the bacterial surface with minimal sample preparation. For the X-ray fluorescence technique, the aim was to adapt a vacuum compatible liquid cell that could fit a biofilm for XRF measurements. As both X-ray techniques have quite different information depths - a further aim of this study was to measure the concentration depth profile of the investigated biocide in the samples. XPS as a photon-in electron-out technique provides information on depths of up to 50 nm and thus it provides information from very near the surface. XRF as a photon-in photon-out technique has varying information depths of up to several 100's of micrometres. For instance, by varying the excitation energy, or the angle of incidence, the information depth of XRF can be varied within the biofilm, and thus it may allow us to access the vertical concentration depth profile. Using angle resolved excitation and/or variable X-ray excitation energies for XPS, this technique will allow the quantitative investigation of the biocide concentration within the range from 1 nm down to 50 nm. This more surface sensitive technique will provide complementary results to reference-free XRF which, under different angles of incidence, and depending on the X-ray energies is more bulk sensitive - up to hundreds of µm. To establish the analysis of the vertical concentration profile of antibacterial agents as a model, an iodine doped agarose thin film was used.

4.1.3.1 *Near-Ambient Pressure X-ray Photoelectron Spectroscopy*

The stakeholder and company SPECS and the federal institute BAM worked closely together in the field of the Near-Ambient Pressure X-ray Photoelectron Spectroscopy (NAP-XPS). SPECS has been the technological driving force to establish XPS in Near Ambient Pressure (NAP) resulting in the EnviroESCA^{TM} instrument. Within this project new fields of research, for example Biotechnology and Medical Technologies, were successfully addressed.

XPS in general is a widely used technique in surface analysis, providing both qualitative and quantitative information about the sample surface. In XPS an inner-shell electron is excited by an incident X-ray photon, with the ionized atom subsequently emitting photo-electrons which are analysed. The probing depth is typically 5 nm to 10 nm for XPS-measurements with a standard Aluminium Kα X-ray source. The information depth is at the same scale as the phospholipid-membrane and the length of exopolysaccharides anchored to the bacterial surface. The relevant elements – typically carbon, oxygen, nitrogen and phosphorous are easily detected and high-resolution core level spectra reveal details about the binding environment of the atoms.

To prevent the emitted photoelectrons from being scattered by gas-molecules, XPS is traditionally performed in ultra-high vacuum (UHV). This enables a controlled sample environment with minimal contamination, but it puts restrictions on what samples can be measured. Bacteria and biofilms are inherently in a hydrated state, and therefore they are only compatible with ultra-high vacuum after extensive sample preparation, usually involving freeze drying or fast-freezing. With the development of near-ambient pressure XPS (NAP-XPS), bacterial samples can be characterised with minimal sample preparation in various gas environments such as

air and water vapour. While the focus has mainly been on planktonic bacteria harvested from solution for both freeze dried and cryo-preserved bacteria, NAP-XPS provides more flexibility in sample preparation as the samples do not have to be vacuum-compatible. Figure 4 shows a schematic of a NAP-XPS instrument. As a regular XPS-instrument it has an X-ray anode as the radiation source and a hemispherical electron analyser. To enable samples to be analysed in near-ambient pressure, while the sensitive instruments are still under ultra-high vacuum, the X-ray source is separated from the analysis compartment by a silicon nitride window. Further, the first aperture is only 300 µm in diameter and a three-stage differential pumping system separates the sample environment and the electron analyser. With this set-up, planktonic bacteria or biofilms grown on a substrate can be transferred directly from buffer or water-solution to the measurement chamber and characterised in air or water vapour. Measurements of *Escherichia coli* reveal that the carbon-spectrum changes when the conditions change from 11 mbar water vapour to 1 mbar air. (M. Kjaervik, 2018)
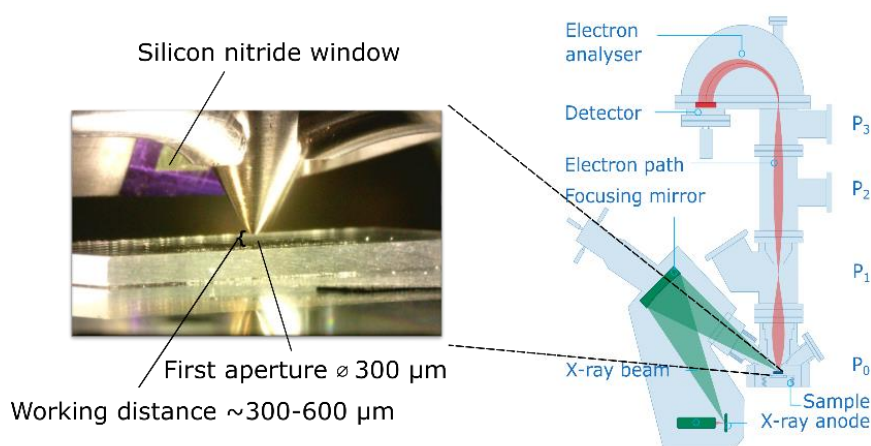

Figure 4 Schematic of an XPS with the typical modifications to adapt it to near-ambient pressure measurements. (Figure is adapted with permission from SPECS)

4.1.3.2 *Surface characterisation of Escherichia coli under various conditions by near-ambient pressure XPS*

The following results from the project are presented in a paper. (M. Kjaervik, 2018) In this paper BAM and SPECS measured *Escherichia coli* (*E. coli*) adhered to silicon wafers under various conditions: in a humid atmosphere at 11 mbar, after drying in the measurement chamber at 2 mbar, pre-dried at 4 mbar, and after overnight pumping at 10^{-4} mbar. The XPS spectra from nitrogen, carbon, and oxygen are presented, and changes in the spectra acquired under different conditions are discussed. *E. coli* K-12 was obtained from the University of Nottingham, UK. Two *E. coli* samples were characterised, both at 2 different pressures. One sample was immediately transferred to the load-lock chamber after being rinsed with PBS and measured in humidity at 11 mbar, the conditions where the bacteria is closest to its natural, hydrated state. It was then gradually dried in the chamber while pumping and it was measured at 2 mbar. The second sample was air dried before it was introduced into the measurement chamber and measured first at 4-mbar air atmosphere, then at 1 mbar after overnight pumping in 10^{-4} mbar, to examine if the dry state influences the *E. coli* XPS spectra.
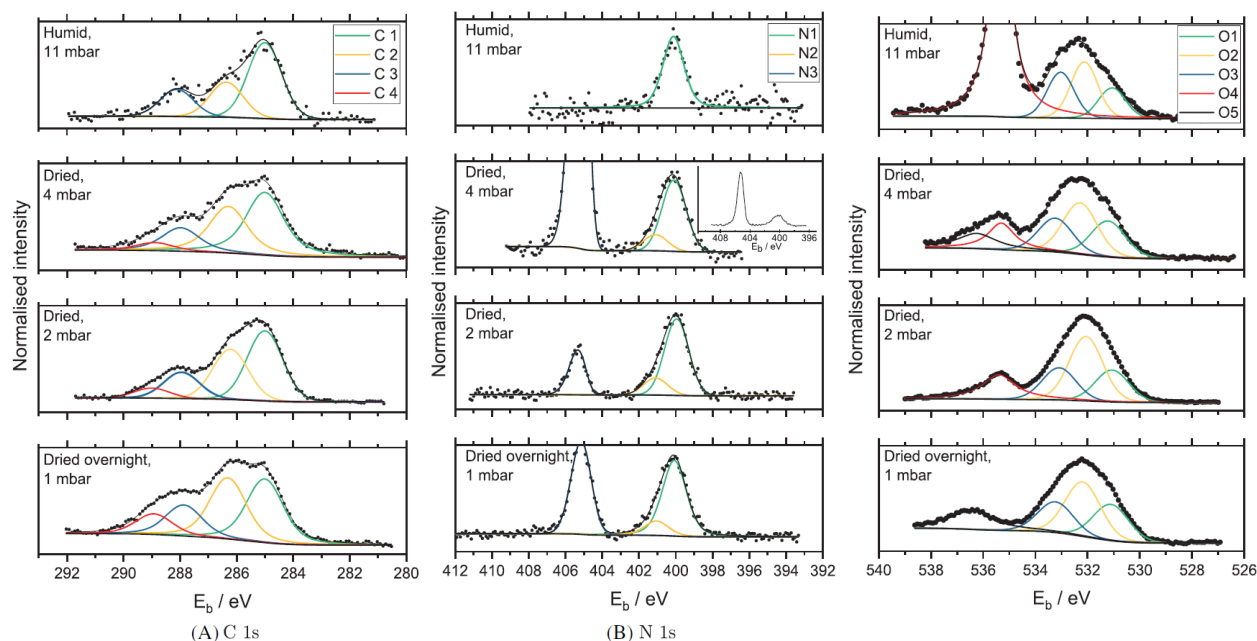
Figure 5. The XPS spectra for A, carbon, B, nitrogen, and C, oxygen acquired under 4 different conditions.

The high-resolution spectra of carbon, nitrogen, and oxygen as depicted in Figure 5 are presented and found to be in general agreement with XPS measurements from freeze-dried and fast-frozen bacteria. However, the amount of carbon components associated with polysaccharides increased relative to aliphatic carbon during drying and it increased further after overnight pumping. This implies that drying has an impact on the bacterial surface. Further experiments were done on different artificial biofilms and biological samples. The sample preparation was supported by NPL and UNOTT.

4.1.3.3   Reference-free X-ray spectrometry

In X-Ray Spectrometry (XRS) an inner-shell electron is excited by an incident X-ray photon, with the ionized atom subsequently emitting a fluorescence photon. Based thereon X-Ray Fluorescence (XRF) analysis is a well-established non-destructive and multi-elemental analytical technique in various fields of applications ranging from materials science and semiconductor characterisation to geology and environmental issues as well as the investigation of biological specimens. The emitted photon's energy is specific to each outer-shell electron's transition to the inner-shell vacancy. Thereby, the emitted fluorescence radiation is characteristic for the element and it can be identified by X-ray detectors which can be either an energy dispersive detector (e.g. Si(Li) detectors or Silicon Drift Detectors) or a wavelength dispersive spectrometer using a grating or a crystal as the dispersive element. The concentration or mass deposition of the elements can then be determined by a quantification model evaluating the intensity of the characteristic fluorescence radiation detected (B. Beckhoff, 2006). Here, typically a calibration procedure is needed for the quantification using a reference material or a dedicated calibration sample leading to traceability in chemical analysis. Ideally, the calibration sample or samples should be very similar to the sample of interest. This prevents quantification aberration induced by non-linear matrix effects which are associated, for example, with (X-ray) absorption effects or secondary enhancement effects by photo electrons. Especially when dealing with biological samples as a light matrix this can become a major issue.

As a modified routine of XRF analysis even reference-free XRS can be applied (Beckhoff, 2008) (C. Streeck, 2018) which is a unique technique developed and operated by PTB. Here, physical traceability is established using radiometrically calibrated instrumentation e.g. well-known X-ray sources and detectors, as well as knowledge on atomic fundamental parameters for the quantification (B. Beckhoff e. a., 2009). Reference-free XRS does not only contribute to the analysis of surface contamination, but also to the assessment of the thickness and composition of micro- and nanolayers as well as to the composition of bulk specimens. Generally, as XRS is strictly an elemental sensitive technique, sample preparation as well as a pre-planning of the series of experiments, is key for a successful measurement campaign. For example, if sample

preparation adds an element to a system in which the same element is present and to be studied, there will most likely be a deteriorated contrast dependent of the concentration of the additive. Furthermore, analysing the uptake of a biocide or antibiotic, e.g. Triclosan, a chlorine containing antibacterial agent found in many consumer and personal health-care products and used for surgical cleaning treatments, in a bacterial biofilm can be complicated, as chlorine is also present as an ion in biological systems.

4.1.3.4   XRS measurements with a novel liquid cell

First in situ-measurements of biomaterial containing liquids in a newly developed liquid cell were successfully carried out by means of reference-free X-ray fluorescence by PTB. The design of the cell is described in the paper of Grötzsch et al. (D. Grötzsch, 2017). The measurement principle and the picture of the cell are shown in Figure 6.
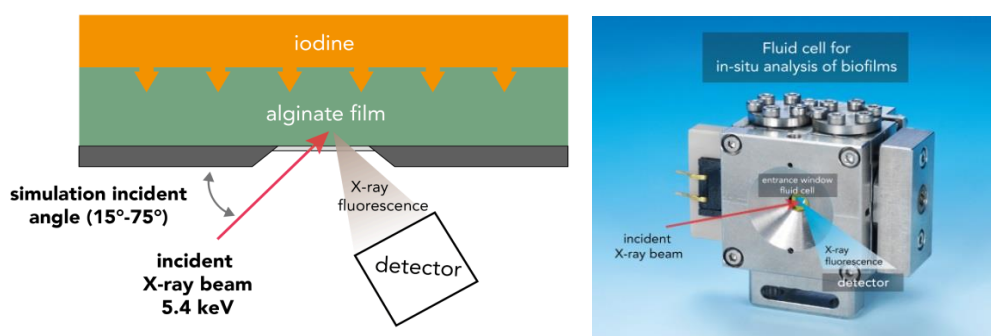

Figure 6. Measurement principle and a picture of the vacuum compatible liquid-cell.

Using X-ray absorption fine structure (XAFS) analysis, PTB have characterised the haemoglobin microparticles with respect to their ration of functional, i.e. the sum of oxyHb and deoxyHb, and metHb content as this technique is sensitive to the chemical bonding to neighbouring atoms and the chemical state of an element of interest. The ratio of oxyHbMP and metHbMP can be estimated by subtracting the scaled metHbMP data from the data obtained on the oxyHbMP sample. The applied criterion is a smooth run of the curve in the region of the Fe^{3+} L_3 resonance. The resulting curves are shown on the right in Figure 7 (blue and purple curves). Here, the metHbMP fraction was estimated to be 35 %.

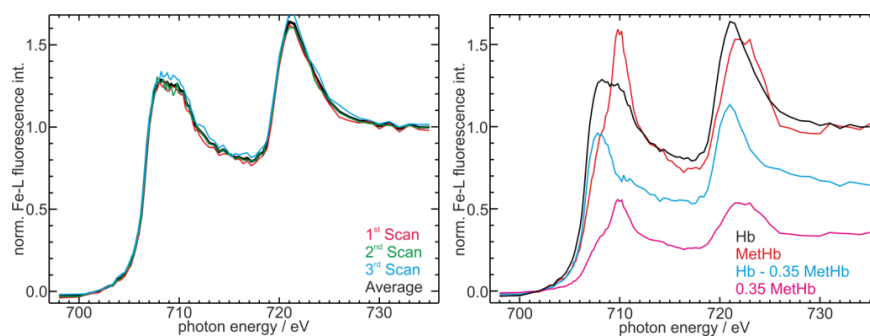**Figure 7. Resulting Fe-L3,L2 NEXAFS obtained from the soft X-ray absorption spectroscopy experiments. On the left, three repetitions as well as the average signal on the oxyHbMP are shown. On the right, the average signals for the oxyHbMP (black), the metHbMP (red) as well as a linear combination to separate the different contributions (blue and purple) within the oxyHbMP signal are shown.**

4.1.3.5   Elemental depth profiling by means of XRS

Elemental depth profiling by means of GIXRF enables the analysis of buried nanolayers and interfaces from a few to several hundreds of nanometres below the surface, thus it also enables depth profiling of a specific element of a biocide or antibiotic in a biofilm. Here different path lengths and thus different absorptions of the X-rays through a material provide information about the buried elements that emitted the X-rays. This absorption is energy dependent, so an element's L-lines will be absorbed differently even though the path length is the same - with the higher energy photons suffering less absorption. This can then be used to calculate the depth of the element of interest.

XRF measurements were carried out by PTB using their Dipole White Light (DWL) beamline at the synchrotron radiation facility BESSY II. Using this polychromatic excitation with an angle of incidence of 45°, a Celgard separator soaked in a 10 % solution of PVP-iodine was buried below an 8 µm HOPG foil. Here the absorption difference of iodine L-line intensities was studied. As Figure 8 shows, the absorption difference of iodine L-lines was clearly visible which means that iodine in a bacterial film of 10 µm thickness can potentially be determined. With the restriction that the absorption in a biofilm in a liquid cell can potentially be an order of magnitude smaller than in a HOPG foil. This can potentially be overcome by realising small exiting angles for achieving longer path lengths.
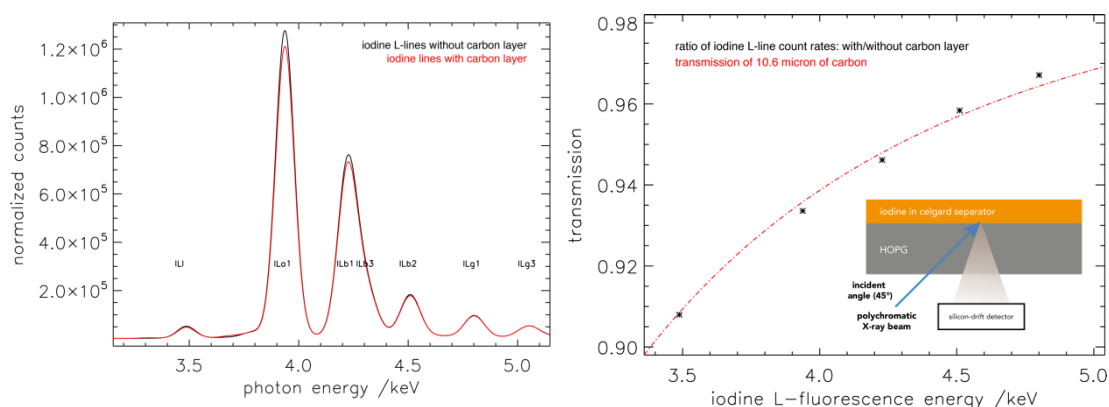

Figure 8. Energy dependent absorption of iodine L-lines in an organic-like carbon matrix.

4.1.3.6   Conclusions

PTB, BAM and SPECS demonstrated that X-ray techniques such as XPS and XRF are appropriate techniques for studying the concentration and uptake of antibacterial agents in bacterial samples and biofilms. BAM and SPECS have successfully performed several studies on artificial and bacterial biofilms and individual bacteria using NAP-XPS. This technique allows us to study biological materials in their natural environment as it does not need to be vacuum compatible any more. XPS and NAP-XPS are very surface sensitive techniques and information on first 10's of nanometres is given. For the first time the XPS spectra of *Escherichia coli* where systematically studied when the water vapour conditions change from 11 mbar to 1 mbar air.

First in situ-measurements of biomaterial containing liquids in a newly developed liquid cell were successfully carried out by means of reference-free X-ray fluorescence by PTB. Using Celgard separators and HOPG foils, both prepared with iodine - an effective biocide - the absorption difference of iodine L-line intensities was studied to analyse the concentration and concentration depth profile of iodine in a bacterial film. For future experiments it will be necessary to take into account that the absorption in a biofilm in a liquid cell can potentially be an order of magnitude smaller than in a HOPG foil or Celgard. This can potentially be overcome by realising small exiting angles for achieving longer path lengths.

4.1.4   Imaging of surface macromolecules and real-time measurements

To develop urgently needed new metrological capabilities for the imaging of surface macromolecules, such as porins or metal-transport proteins, to study the efflux mechanisms in Gram-negative bacteria and to give real-time quantitative measurements of drug-uptake in bacteria and biofilms. Numerical modelling and algorithms will be developed to support measurements in complex biological environments.

Two different optical strategies to study the interaction and localisation of drugs in bacteria and biofilms were developed during the project. In particular, a super-resolution microscopy platform for single-molecule localisation in bacteria and a microfluidic Raman-DEP (dielectrophoretic) device to follow dynamic interactions of the bacteria with antibiotics were developed by LENS and INRIM, respectively, both with the support of UNOTT for the standard microbiology. The super-resolution microscopy platform was validated by performing the super-resolution imaging of fluorescent antibiotics on the surface of bacteria and of the bacterial proteins (efflux pumps) involved in antimicrobial resistance, both in planktonic cells and in biofilms. Alongside the microscopy platform, an engineered strain of the bacterium *E. coli* was developed in which the efflux pump component AcrB is labelled with a fluorescent protein that is suitable for Photoactivated Localisation Microscopy (PALM). This enabled us to obtain quantitative data on the expression and distribution of this well-studied protein with an unprecedented level of detail. Moreover, a microfluidic device based on the combination on Raman-DEP techniques was developed to detect dynamic changes in the Raman bacterial profile during drug susceptibility testing. This procedure allowed us to obtain direct, real-time measurements of a suspension of planktonic bacteria without labelling or other time-consuming sample preparation processes. The present methodology was validated by testing *E. coli* susceptibility towards ciprofloxacin by monitoring spectral changes in the chemical fingerprint of the bacteria over a 3-hour time span. Raman data processed with supervised multivariate data analysis were able to show the detection of subtle spectral differences at a molecular level between treated or untreated bacterial cells after only 1 hour of treatment.

In the following paragraphs, both approaches are described in detail showing the main achievement and advantages of both techniques.

4.1.4.1 *Super-resolution microscopy platform for single-molecule localization in bacteria and biofilms*

The aim was to investigate bacterial macromolecules and their interaction with antibiotics through single-molecule localisation techniques, both in planktonic bacteria and in biofilms. When bacteria switch from a planktonic to a biofilm-associated lifestyle, a wide remodelling of gene expression takes place. In particular, efflux pump genes such as the acrAB operon are known to be upregulated under biofilm growth when compared to planktonic bacteria, and this phenomenon plays an important role in determining an increased resistance of biofilms to antimicrobial treatments. Although efflux pump expression in biofilms has been previously investigated through indirect methods, direct observation and quantification of efflux pumps at the single-cell level has never been reported to our knowledge. Here a method involving CRISPR/Cas9-assisted genome editing coupled to single-molecule localisation microscopy was implemented to obtain quantitative data on the expression and distribution of the AcrB efflux pump in both planktonic and biofilm-associated *Escherichia coli* cells.

An *E. coli* BW25113 strain was engineered with a chromosomally encoded fusion between the native *AcrB* gene and the coding sequence for PAmCherry, a photoactivatable fluorescent protein (F.V. Subach, 2009). The functionality of the fluorescently labelled AcrB protein was verified by measuring the MIC of chloramphenicol, an antibiotic which is a specific substrate of AcrB, via the microdilution method in LB medium (Clinical and Laboratory Standards Institute, 2012). The minimum inhibitory concentration (MIC) for both the acrB-PAmCherry strain and the control wild type (WT) strain was measured at 8 µg/ml while the MIC for both deletion mutants was 2 µg/ml. The PALM (PhotoActivated Localisation Microscopy) super-resolution microscopy technique (Hess, 2006) was used to directly visualise and count individual instances of AcrB on planktonic bacteria before and after exposure to an antibiotic, as well as within fully-grown biofilms. PALM relies on the FIONA (Fluorescence Imaging with One Nanometre Accuracy) principle by Selvin et al. (Selvin, 2007), and it employs chemical control over fluorophore photophysics to resolve the position of individual fluorescent molecules in a crowded environment. By using photo-activatable fluorescent proteins, it is possible to stochastically excite only a small fraction of the fluorophores in a sample and to resolve them individually. By performing this operation for several thousands of frames and localising the centre of each point spread function with the FIONA method, it is possible to obtain a detailed and complete map of the fluorescently labelled proteins with an accuracy of a few nanometres.

As with all single-molecule localisation methods, PALM is a widefield microscopy technique that needs high acquisition speeds and high signal-to-background ratios in order to provide the best results; as such, limiting the background fluorescence originating from out-of-focus planes is of crucial importance. Optimised illumination techniques such as Highly Inclined and Laminated Optical sheet (HILO) microscopy (Tokunaga, 2008) provide the means to perform widefield image acquisition whilst keeping the out-of-focus fluorescence low (Vignolini, 2018) (Vignolini T. G., 2018). LENS, together with the support of UNOTT, developed a

combination of PALM and HILO to count and localise with high precision the AcrB-PAmCherry fusion proteins expressed by *E. coli* when grown to mid-log phase in the absence of antibiotics, and after different times of exposure to sub-inhibitory concentrations of chloramphenicol.

PALM microscopy was performed on fixed bacteria on a custom-made microscopy setup by using a 405 nm laser to switch the activation of individual PAmCherry molecules and a 532 nm laser to excite fluorescence. Images were taken until complete photobleaching of PAmCherry was observed. Raw image stacks were analysed with the ThunderSTORM ImageJ plugin (Ovesný, 2014) in order to reconstruct super-resolved molecular maps such as the one shown in Figure 9.
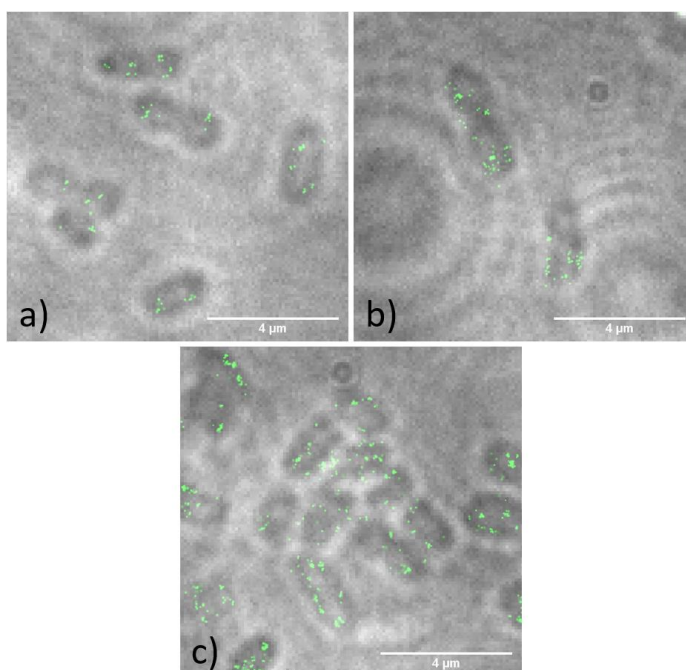
Figure 9. Super-resolution maps of AcrB-PAmCherry after a) no exposure, b) 40 minutes of exposure and c) 80 minutes of exposure to chloramphenicol.

The same technique was used to perform super-resolution imaging of AcrB in live *E. coli* biofilms. Bacteria were inoculated in glass-bottomed chambers containing sterile M9 minimal medium with added glucose, then they were left to grow for >24 h at 37 °C with no agitation, and then directly imaged in the same medium without mechanically perturbing the biofilm. Figure 10 is an example of a super-resolved image of AcrB obtained in a biofilm.

Figure 10. Super-resolution map of AcrB-PAmCherry in a biofilm.

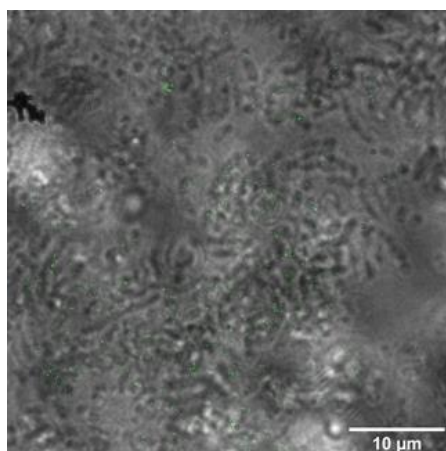In summary, a method was developed that allows us to directly localise and quantify expressed proteins on both isolated bacteria and complex biofilm environments. By using state-of-the-art genome editing techniques which minimise unwanted transcriptional and translational side effects on labelled proteins, and by taking advantage of the quantitative nature of single-molecule localisation techniques, protein expression and distribution in single bacterial cells was observed with unprecedented accuracy. The method was demonstrated by the successful imaging of the AcrB efflux pump. The technique presented here will allow us to extract valuable data on the regulation of antibiotic resistance systems in bacteria, and to investigate the still largely unexplored differentiation of isogenic bacteria in the biofilm environment.

4.1.4.2 *A microfluidic Raman-DEP (dielectrophoretic) device to follow dynamic interactions of bacteria with antibiotics*

The aim was to develop a procedure to detect changes in the Raman bacterial profile during drug susceptibility testing with various implementations. The Raman spectroscopic and dielectrophoretic (DEP) approaches were combined to obtain direct, real-time measurements of a suspension of planktonic bacteria without the need for any labelling or other time-consuming sample preparation processes. The technique was applied to test *Escherichia coli* susceptibility towards ciprofloxacin by monitoring spectral changes in the chemical fingerprint of the bacteria over a 3-hour time span. The present methodology was developed by INRIM with the support of UNOTT for the standard microbiology.

4.1.4.2.1 *Measurement system*

Dielectrophoresis is a phenomenon that describes the movement of dielectric particles when subjected to a non-uniform electric field. The basis for generating the DEP force is the interaction between the particle's dipole and the spatial gradient of the electric field. Raman analysis on dispersed bacteria can be difficult to achieve, but using DEP with appropriate voltage and frequency, bacterial cells could be manipulated into clusters to increase their local concentration in order to optimise the Raman signal to noise ratio (Schröder, 2013). The integrated dielectrophoresis Raman setup consists of a sample holder that contains a chip made of a quartz glass substrate coated with gold microelectrodes that generate the non-uniform electric field which provides the DEP effects. Bacteria in a liquid medium with known conductivity are injected in the transparent window of the device, between the cover glass, the gasket and the chip. A sinusoidal voltage, predetermined in amplitude and frequency to maximise bacterial agglomeration without noticeable sample heating or damage, is applied to the electrodes. When bacteria are gathered, the Raman spectra are acquired using a water immersion objective (Figure 11).
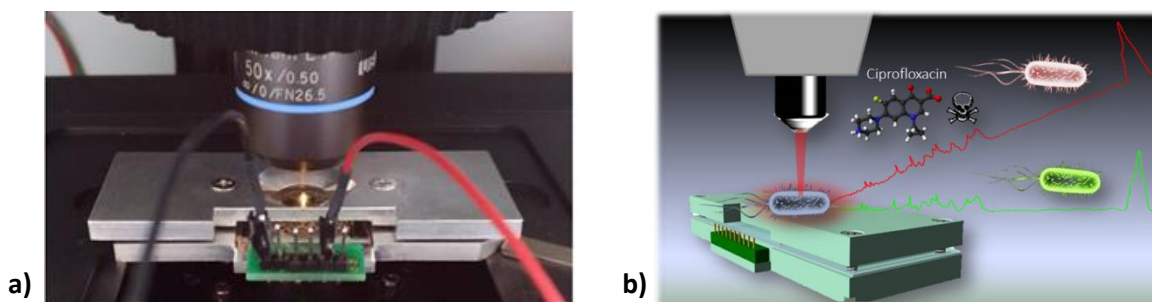

Figure 11. a) The sample holder is placed under the microscope objective and connected to the voltage source. b) Simplified scheme of the application of the Raman-DEP to study *E. coli MG1655* Raman spectral changes of untreated (green spectrum) and treated samples with ciprofloxacin (red spectrum).

4.1.4.2.2 *Results and development of statistical analysis*

The combined Raman-DEP technique was applied to test the susceptibility of *E. coli* to the commonly prescribed second-generation fluoroquinolone ciprofloxacin (CP), by monitoring spectral changes in the chemical fingerprint of the bacteria, which are related to the mode of action of the drug. *E. coli MG1655*, a non-muted strain of *Escherichia coli* which is sensitive to ciprofloxacin was chosen.

The MIC (minimum inhibitory concentration) and the MBC (minimum bactericidal concentration) of ciprofloxacin towards *E. coli MG1655* were investigated by performing both broth microdilution and a colony forming units (CFU) assay as described by the National Committee for the Control of Laboratory Standards

guidelines (NCCLS, 2007). The MIC and MBC of ciprofloxacin for *E. coli* MG1655 were assessed to be 0.5 µg/ml and 1µg/ml, respectively.

Raman analyses were then performed using the Raman-DEP setup. Comparisons between bacterial treated and untreated samples (CTRL) were performed at MBC (1 µg/ml) and high sub-MIC levels (0.015 µg/ml) of ciprofloxacin for different time points over a 3-hour time span. Simultaneously, standard microbiological assays based on cell viability, turbidity tests and fluorescence microscopy, were carried out as reference methods to correlate the observed Raman response. Differences between the spectra of CTRL and Treated bacteria were detected (Figure 12a).

Even though the spectral profile of control and treated samples are very similar, statistical differentiation due to minor changes which are dependent on drug treatment were highlighted by exploring Raman data with Principal Component Analysis (Figure 12b), which helps in the visualisation of non-random variation in spectral data.
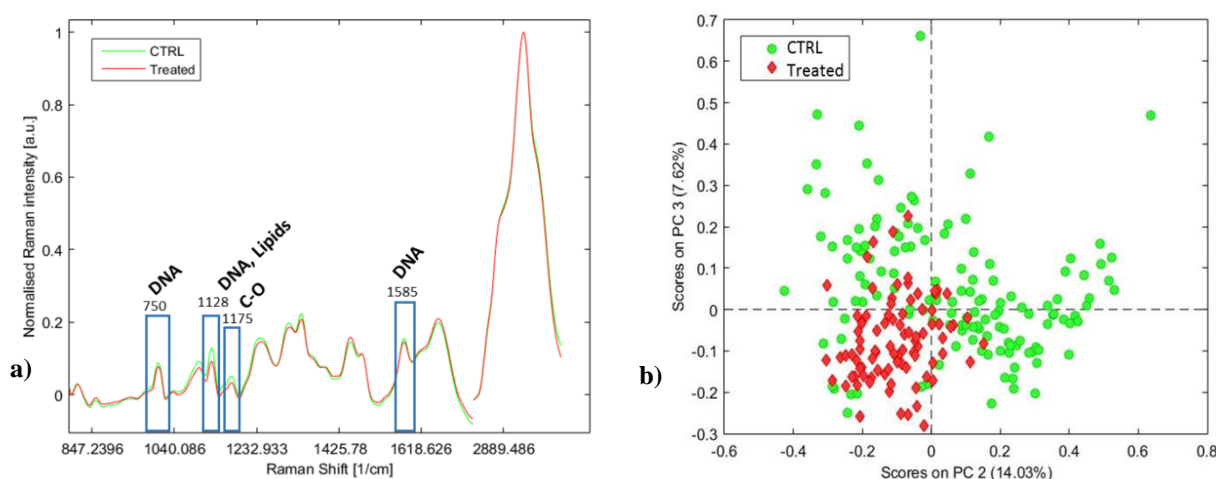

Figure 12. a) Raman average spectra of *E. coli MG1655* untreated (green) and treated with 1 µg/ml of ciprofloxacin for 1 hour (red). A chemical meaning was assigned at the bands where major differences were highlighted. b) Principal Component Analysis of CTRL sample (green) and test (red) where each point represents one Raman spectrum.

PCA, which permits the easier visualisation of similarities between spectra and to identify the unsupervised grouping of data based on the directions of maximum variance (PCs), revealed that Raman spectra captured changes related to the antibiotic treatment. In the PCA score plot (Figure 12b) it is very easy to see that PC2 and PC3 separate the controls from the treated ones quite well after only one hour of treatment with the antibiotic. Statistical analyses helped us find the spectral regions of maximum variance, which were focused on to make a spectral analysis on the bands that changed the most between Treated and CTRL samples. As ciprofloxacin targets cellular DNA, it was not surprising to find that the signals that vary the most after the antibiotic treatment were those corresponding to the vibrational modes of nucleic acids (Figure 12a). In particular, spectral changes were found in the band at 1585 cm^{-1} that corresponds to v_{C-N}, δ_{N-H} of guanine and adenine; in the peak at 750 cm^{-1} corresponding to v_{O-P-O} and the aromatic ring vibration of nucleic acid; and in the bands at 1128 cm^{-1} and 1178 cm^{-1} due to the C-O stretching modes of the saccharide components of the lipid, DNA and RNA backbones (Kloß S, 2013).

PCA analysis showed that the passage of time has some effects on the chemical structure of bacteria in both CTRL and Treated samples (Figure 13a & b). This can be seen in different spectral regions by the comparison of the spectra from the CTRL and the ones treated with the antibiotic. The score plot of Figure 13b shows that PC 1 and PC 3 demonstrate a spectral variance dependent on time. In fact, the spectra obtained at each different time point of the treatment are quite well separated from each other especially from time 0 (green) to time 1 (yellow) and there is a quite ordered descending trend along the two PCs. In the score plot of Figure 13b PC 1 and PC 3 show a spectral variance that is dependent on time. In fact, spectra obtained at each different time point of treatment are quite well separated from each other especially from time 0 (green) to time

1 (yellow) and there is a quite ordered descending trend along the two PCs. Therefore, a Partial Least Square-Discriminant Analysis (PLS-DA) model was used to classify the Raman spectra of bacteria according to their response to antibiotic treatment, one PLS-DA model for each time point was built, so their efficacy was higher than that of a total classification (Figure 14).
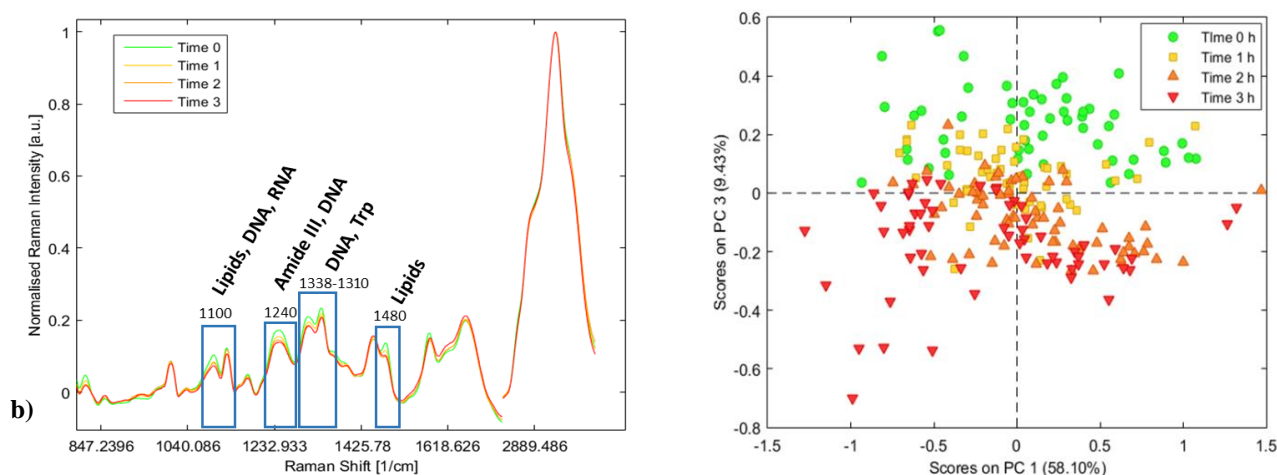

Figure 13 a) Raman average spectra of *E. coli MG1655* treated for 0 hour (green), 1 hour (yellow), 2 hours (orange) and 3 hours (red) with 1 µg/ml of ciprofloxacin. A chemical meaning was assigned at the bands where major differences were highlighted. b) Principal Component Analysis of Raman data obtained from the samples described in Fig. 13a where each point represents one Raman spectrum.

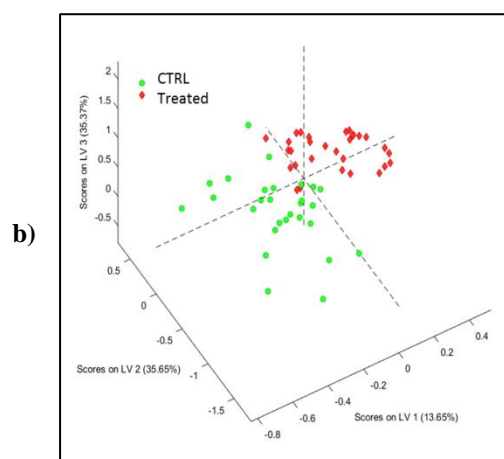|	1 h	2 h	3 h
Sensitivity (Prediction)	0.67	1.00	1.00
Specificity (Prediction)	1.00	0.50	0.33
Class. Error (Prediction)	0.17	0.25	0.33

Figure 14. a) Table of sensitivity, specificity and classification error of PLS-DA models built for each time point b) PLS-DA model built on Raman data of six independent experiments of *E. coli MG1655* untreated (green) and treated with 1 µg/ml of ciprofloxacin for 1 hour (red).

From the PLS-DA (Figure 14a) it is evident that the error rate increases over time while the specificity of the prediction decreases due to the fact that the effect of treatment adds up to that of time. Therefore, the focus was on time 1 (1 hour of treatment with ciprofloxacin) where major differences between treated and untreated samples were highlighted (Figure 14b). Each supervised model was built on six independent experiments, five were used for training and one for the validation.

In order to test the predictive strength of our statistical model, the same experiment described above was repeated using a concentration of ciprofloxacin of 0.015 µg/ml, which is more than 100 times under the MIC for *E. coli MG1655* in our experimental conditions. As ciprofloxacin is a bactericidal drug that inhibits DNA gyrase and topoisomerase IV (enzymes necessary to separate bacterial DNA), thereby blocking cell division (Fisher L. M., 1989), the OD_{600nm} test performed at the MIC concentration showed that bacteria stop their

growth after one hour of treatment (the time necessary to have at least two complete cycles of bacterial replications and to the drug to exploit its effects on the total population of cells). On the other hand, bacteria treated with 0.015 µg/ml continued their growth, even if more slowly than the untreated controls (Figure 15a). The developed PLS-DA model was used to predict the classification of the spectra obtained from the sample of *E. coli* treated with 0.015 µg/ml of ciprofloxacin in order to see whether the sample can be classified as a control or treated (Figure 15b).

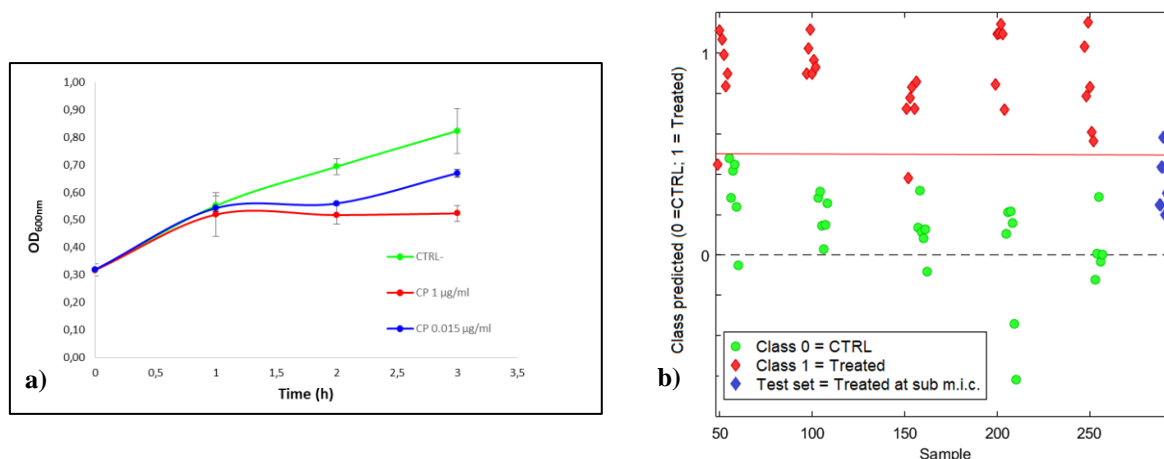**Figure 15 a) Growth curves of *E. coli MG1655* (OD$_{600}$ vs time) for untreated (green), treated with 1 µg/ml (red) and 0.015 µg/ml (blue) of ciprofloxacin. b) PLS-DA model for the classification of the *E. coli MG1655* Raman spectra using untreated (green), treated with 1 µg/ml (red) and 0.015 µg/ml (blue) of ciprofloxacin after 1 hour of antibiotic treatment. Each point represents one Raman spectrum.**

The results demonstrate that our model is statistically strong and sensitive enough to correctly predict, after just 1 hour of treatment, the susceptibility of *E. coli* to ciprofloxacin when different concentrations at the MIC and sub-MIC level are employed. In order to prove that ciprofloxacin induced effects are already present in *E. coli MG1655* after one hour of treatment, a morphological analysis was performed using Brightfield and Fluorescence Microscopy, confirming that that ciprofloxacin produces some effects on the morphology of *E. coli MG1655* just after one hour of treatment (data not shown).

4.1.4.2.3 *Summary*

The developed Raman-DEP device allows the characterisation of different bacterial strains with high specificity and the following of dynamic interactions of the bacteria with antibiotics. Raman data processed with supervised multivariate data analysis are able to detect subtle spectral differences at a molecular level between treated or untreated bacterial cells after only 1 hour of treatment. The importance of the combined Raman-DEP method is clear because it could open the way to rapid bacterial antibiotic susceptibility testing without the necessity of the time-consuming sample preparation and overnight incubation required by classical microbiological techniques.

4.2   *Objective 2*

To develop well-controlled model systems to allow cross-platform measurement of penetration, accumulation and efflux of antibacterial agents in single cells, in suspended cellular aggregates, as well as in biofilm communities including binding to biofilm matrix components. The efficacy of novel antibacterial agents and efflux pump inhibitors will be investigated.

Well-controlled model systems are relevant to the project to enable the different platforms to measure antimicrobial agents consistently in a way that can be compared across them. This is important in order to deliver the objectives of assessing where and to what extent antimicrobial agents accumulate in single bacterial cells and biofilm communities. It is necessary to determine whether novel antibacterials are efficacious in this context because novel antibacterial agents are currently tested with single cells, but biofilms are the predominate bacterial growth form, and are more resistant to antibacterials.

4.2.1 *Bacterial model system*

Bacterial model systems were developed by UNOTT, based on the discussions with all partners. This objective was achieved as biofilm models were developed that could be successfully imaged by OrbiSIMS (NPL), Nano-SIMS (NPL) and also Raman spectroscopy (PTB, INRIM). Molecules of interest, including antimicrobials, were detected and quantified. For example, Triclosan and Ciprofloxacin were detected within bacteria by Raman Microscopy. As a measure of efficacy, fluorescent microscopy (with or without confocal analysis) monitored the rate of bacterial death within biofilms, which correlated with the concentration of antimicrobial. This analysis was undertaken using the model bacterium *Pseudomonas aeruginosa*, and the antimicrobials ciprofloxacin, tobramycin and benzalkonium chloride. In addition, analysis of *Staphylococcus aureus* provided supporting evidence with triclosan alone or in combination with a range of antibiotics including ciprofloxacin and vancomycin. The optimised protocols were used by UNOTT and NPL to evaluate antimicrobially resistant strains of the bacterium *Pseudomonas aeruginosa* (deficient in Mex efflux pumps) to see if they accumulated antimicrobials, and more microcolonies of a similar structure were observed to form within the biofilms.

Three case studies, agreed by the consortium, were selected to assess the penetration of antimicrobial agents. One used novel antagonists/agonists that target bacterial cell-cell communication, one tracked the antimicrobial iodine, and one investigated how triclosan affects resistance to other antimicrobials. The bacterial cell-cell communication inhibitor reduced biofilm formation by *Pseudomonas aeruginosa* in the flow cell and also reduced the number of viable bacteria within static biofilms when encapsulated in alginate nanoparticles. Iodine penetrated into biofilms formed on top of skin *in vitro* to reduce their viability. The pre-treatment of bacteria with triclosan induced tolerance against the antibiotics ciprofloxacin and vancomycin when they were free living, and also when in a biofilm, and it was revealed that the underlying molecular mechanism involves the stringent response and an overproduction of extracellular polysaccharide. Raman spectroscopy was used to follow this in *Escherichia coli* as well.

A

B

C

PAO1 expressing **GFP (live)** and stained with **PI (dead)**

PAO1 expressing **GFP (live)** and stained with **PI (dead)** + 1 ug.ml⁻¹ ciprofloxacin
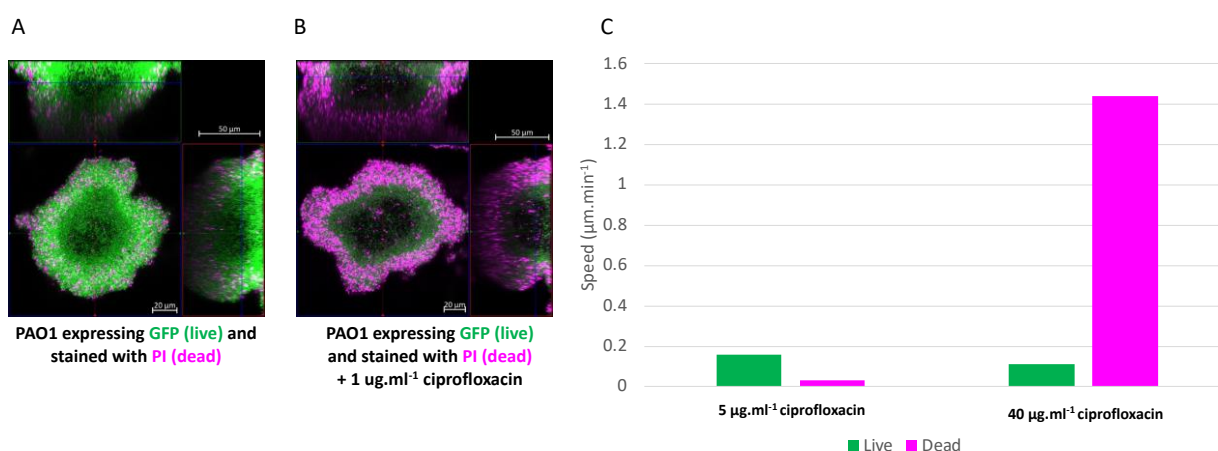
Figure 16. *Pseudomonas aeruginosa* was grown as a biofilm in a bioflux and exposed to the DNA gyrase inhibitor ciprofloxacin at the concentrations indicated. Live bacteria were green due to fluorescence from the Green Fluorescent Protein (GFP) they produce. Dead cells were stained with propidium iodide. The bacteria around the outside of microcolonies died first (panels A and B) and the rate of death was faster with a higher concentration of ciprofloxacin (panel C).

4.2.2 *Artificial biofilm model*

The aim was to develop an artificial biofilm model system to allow partners, including NPL, PTB, BAM, SPECS, INRIM and LENS, to perform a metrological intercomparison of the vertical concentration profiles of antimicrobial compound distribution in the biofilm by the analytical platforms developed in the project. In addition, the artificial biofilm could serve as a reference sample in VAMAS interlaboratory comparisons.

4.2.2.1 *Model system*

Alginate was chosen by the consortium as the main component of the artificial biofilm. Alginate is inexpensive and safe to handle. It is also an exopolysaccharide component of the biofilms produced by the Gram-negative

bacterium *Pseudomonas aeruginosa.* Iodine was chosen as the antimicrobial agent. Iodine is a well-known antimicrobial compound, used, for example, in wound dressings to prevent wound infections. Iodine is a unique element which is absent in biological samples. In addition, it can be easily detected and identified by analytical techniques such as GI-XRF, SIMS, Raman and NAP-XPS. Several different substrates were tested to accommodate the requirements of all the partners and their different analytical platforms. The tested substrates included a sapphire disk, a calcium fluoride wafer, and a silicon wafer.

To facilitate the efficient and stable attachment of the alginate to the substrate surfaces, a protocol for surface functionalisation by silanation was developed. The artificial biofilm sample is prepared by spin-casting the alginate containing iodine onto a cleaned and silanised substrate. Before the spin-casting, iodine is added to the alginate solution at the final concentrations of either 0.09 % (w/w) or 0.009 % (w/w). Air-dried artificial-biofilm samples are then kept in the dark, at room temperature in a desiccator.

4.2.2.2 Sample assessment

In-batch repeatability of sample preparation was tested by NPL. A range of samples was prepared using the same stock solution of alginate - iodine mix and the same sample preparation protocol. Samples with two different contents of iodine (of either 0.09 % (w/w) or 0.009 % (w/w)) were tested. The samples were measured by secondary ion mass spectrometry (SIMS) depth profiling and by atomic force mass spectrometry (AFM).

▪ The average film thickness measured by AFM was 6.20 µm ± 14 % (n = 10).

▪ The vertical profiles through the samples measured by SIMS showed an excellent uniform distribution of iodine through the entire sample depth with an average relative standard deviation of 2.13 % (n = 22). See the example of the artificial-biofilm depth profile in Figure 17.

▪ The differences in the relative amount of iodine between different sample areas as well as between different samples was estimated based on the ratio of the intensities of the iodine ion (m/z 126) and one characteristic alginate ion (m/z 71). For that, the ion intensities from 60 data points from each depth profile plateau region were summed. Planar inhomogeneity was observed with a significant standard deviation of > 80 % for both iodine concentrations (n = 18 for 0.09 % iodine (w/w) and n = 6 for 0.009 % iodine (w/w)). An example of surface inhomogeneity is illustrated in Figure 18.

Two different sample storage types were tested including storage in a desiccator at room temperature and storage in a fridge at 4 ˚C. The effect of the high vacuum of the SIMS instrument on the sample was also tested. Three samples from one batch were measured by SIMS depth profiling and AFM and then stored for 2 weeks at the different conditions. After 2 weeks the samples were re-measured. No differences or effects between any of the storage conditions were observed for the samples.

The effects of rehydration of the samples were also considered. The rehydration of the dried artificial biofilm can either be done by either placing the dried biofilm into a container with ultrapure water or by incubation in a high-humidity chamber. After subsequent dehydration of the hydrated samples no changes to the samples were observed. Rehydration does not affect the vertical iodine distribution nor the sample thickness.

The cryopreservation by high-pressure freezing of the alginate films have also been performed, providing satisfactory results.

The planar inhomogeneity was also confirmed with near-ambient pressure X-ray photoelectron spectroscopy (NAP-XPS) carried out by BAM and SPECS and Raman spectroscopic characterisation done by INRIM and PTB (data not shown).
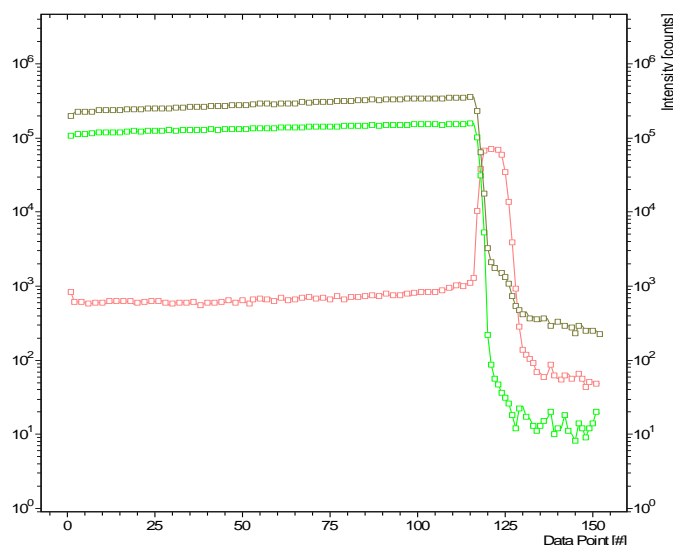
Figure 17. An example of a SIMS depth profile through the artificial biofilm sample. The brown trace corresponds to the iodine ion (m/z 126), the green trace to a characteristic alginate ion (m/z 71) and the red trace to the signal from the sample substrate, SiO_2^- (m/z 60).
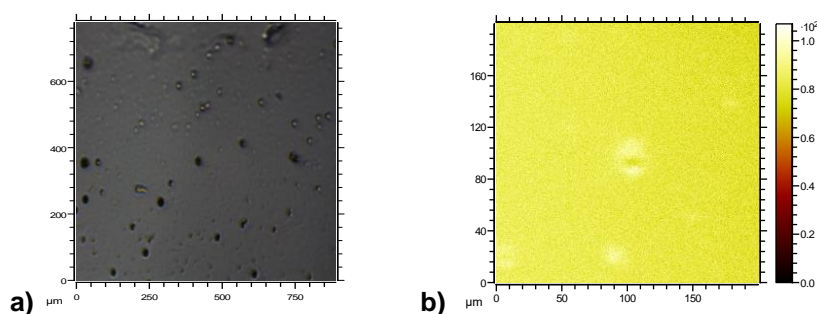

Figure 18. Examples of sample surface inhomogeneity; a) an optical image of a sample surface and b) an image of iodine distribution (m/z 127) in the analysed area of the sample.

Advanced computational methods based on multivariate data analysis of SIMS depth profiles were further used to assess the homogeneity of the vertical iodine distribution within the alginate films, as measured by SIMS depth. Measurements of the entropy of iodine ion images were used as a proxy measure for homogeneity where a high value indicates disorder in the image and a lack of patterns or structure which can be interpreted as uniformity or homogeneity. This was calculated throughout a depth profile of the alginate films containing iodine to compare the homogeneity of iodine through the sample depth. This is shown in Figure 19. The entropy of the iodine ion images is roughly constant until there is an abrupt change at the interface between the alginate film and the substrate. This technique can be used to characterise samples based on levels of homogeneity and depth profile signatures.

The analysis in Figure 20 shows the depth profile on the left panel with ion yields in principal component (PC) space (giving rise to the negative values) versus sputter time, and the ions correlated to that profile on the right panel. For the correlated ions, the magnitude denotes how strongly a given ion is correlated to this profile, and the sign denotes correlation (positive) or anti correlation (negative). PC is correlated with ions relating to the alginate and iodine, and negatively correlated with ions associated with the substrate. PC 2 indicates ions associated with the functionalised (silanised) sample substrate and PC 3 reveals ions that exhibit a strong variation in yield through the depth profile either increasing (positive) or decreasing (negative). High order PCs, such as PC 4 reveal features at the interface layers.
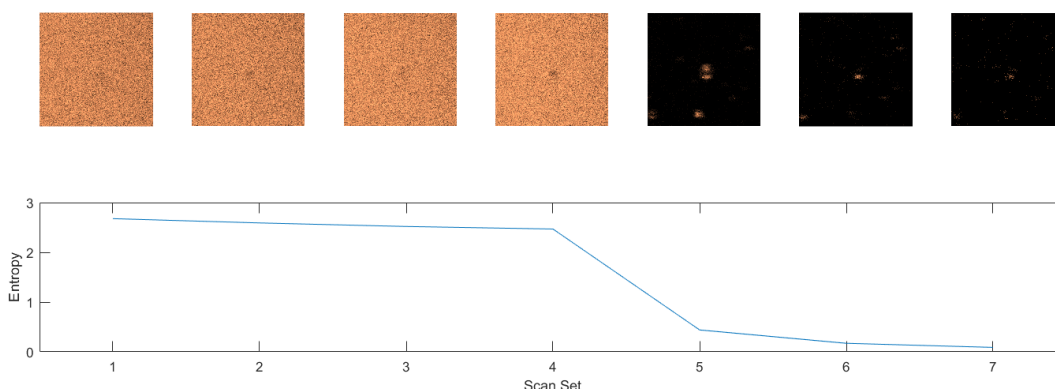
Figure 19. Top ion images of iodine (126.91 m/z) at increasing depths through the sample. Bottom entropy as a measure of homogeneity of iodine though the sample depth.
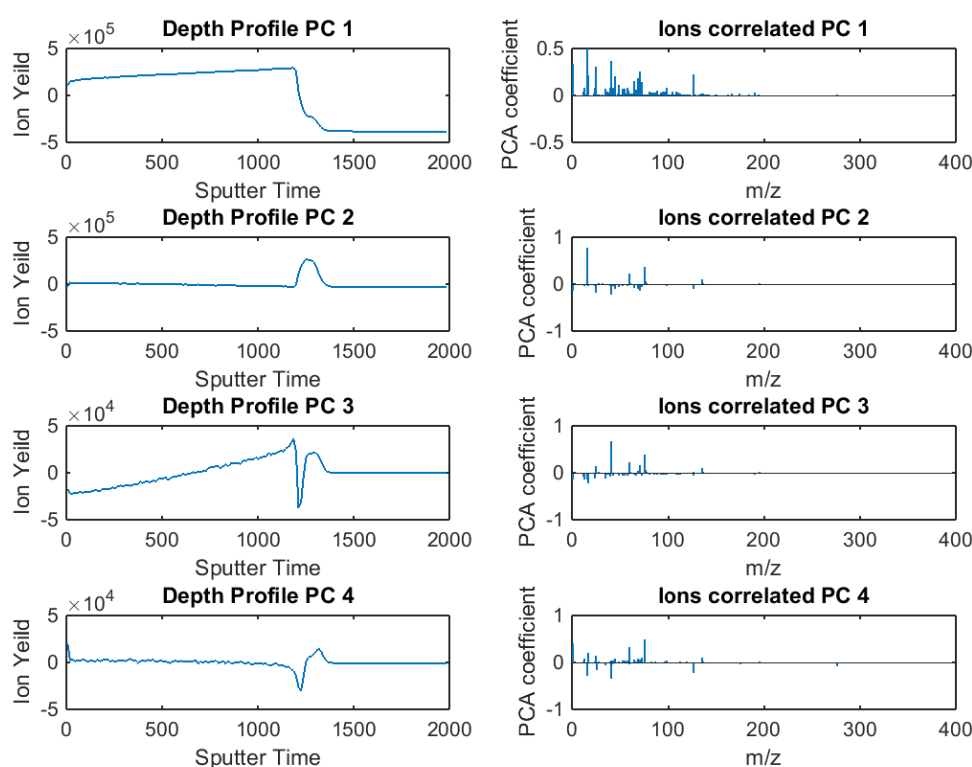

Figure 20. PCA of the depth profile of the alginate biofilms.

4.2.2.3   Conclusion

Based on the measurements of relative to alginate iodine amount, there is a significant planar inhomogeneity of the iodine distribution within a sample as well as significant in-batch variability between the samples. Therefore, the constructed artificial biofilms are not suitable for the round-robin studies, planned between partner-laboratories (NPL, BAM, SPECS, PTB, INRIM and LENS) within the MetVBadBugs project. However, the created model samples could be used as a reference material for the VAMAS interlaboratory study on SIMS depth profiling through frozen hydrated organic materials. SIMS is becoming more and more popular for the analysis of biological samples and the need for the cryo-SIMS capability is also increasing. There are only a few laboratories, which have developed the capability of SIMS analysis of frozen-hydrated materials, providing different solutions to both sample handling and the analysis. A systematic study is necessary to assess the different factors of such an analysis. An example analysis could involve the sputtering yields of ice and the effects the vitreous ice has on the sensitivity of analysis; the effectiveness of sample handling on the

stability of the frozen-hydrated state; depth profiling though frozen-hydrated material using different beams and conditions and their effects on sensitivity. The artificial biofilm created would be well suited to this purpose. The vertical distribution of iodine is constant through the sample depth as analysed by SIMS depth profiling. The sample is stable, safe to handle and can be easily dehydrated and frozen at the place of analysis, hence the shipment of samples under liquid nitrogen conditions can be avoided. The presented multivariate data analysis would be well suited to in-depth analysis of the VAMAS study data.

4.3 Objective 3

To develop signal enhancement strategies and advanced sample preparation methods for studying antibacterial agents in bacteria and biofilms including Advanced cryo preparation methods to enable 'liquid' (vitrified) water to be present in the vacuum of high-performance metrology instruments without ultrastructural reorganisation and translocation of exo/endo -genous molecules; Novel methods to nano-sculpt bacteria for chemical imaging at 50 nm resolution; and nano structured substrates for enhanced sensitivity.

4.3.1 *Cryogenic sample preparation and handling*

DOH, in cooperation with NPL, developed protocols for the freezing of planktonic bacteria and biofilms by high pressure freezing to enable 'liquid,' albeit vitrified, water into the vacuums that are required for high performance metrology instruments. The immobilisation of water in these samples reduces the ultrastructural reorganisation and the loss or translocation of exo/endo -genous molecules, which occurs with dehydration. Complete vitrification of the water within a biological specimen was essential as the formation of ice crystals within a cell can cause disastrous effects on ultrastructure.

High pressure freezing was chosen for biofilm samples as it allows vitrification of the samples up to 500 µm thick. Considerable effort went in to assessing a cryoprotectant that is compatible with SIMS chemical imaging. Cryoprotectants are added to samples to prevent damage that could be caused by the high-pressure freezing process. A range of media were evaluated by NPL and DOH including methanol, bovine serum albumin, dextran and hexadecane. Their presence in the sample had a significant effect on the SIMS spectra, reducing or obscuring the bacterial signal. 150 mM solution of ammonium formate was finally chosen as the most compatible cryoprotectant. Ammonium formate does not interfere with SIMS analysis and is commonly used to wash biological samples from salts, which otherwise have a very strong signal in the mass spectrum and can suppress other ions. Its efficiency as a cryoprotectant, was evaluated by the electron microscopy imaging of frozen-hydrated bacterial samples.

The quality of the vitreous samples was tested by DOH by cryo-TEM and SEM and electron diffraction. Example images of the high-pressure frozen *Pseudomonas aeruginosa* are shown in Figure 21. The electron diffraction pattern additionally confirms the sample to be in vitreous state.
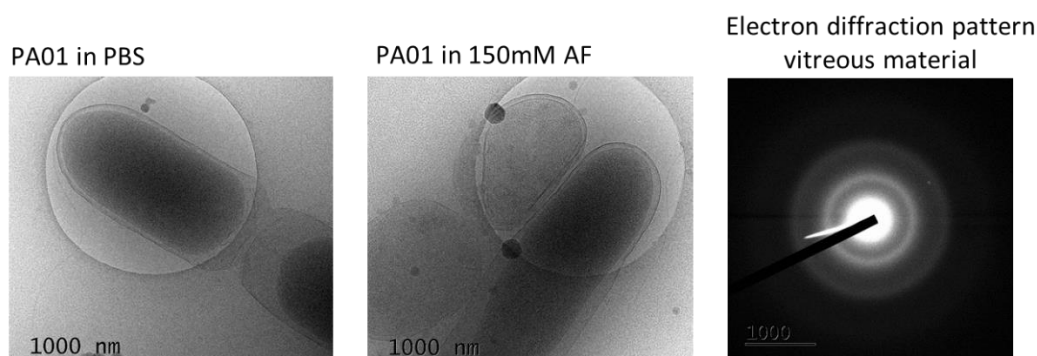
Figure 21. Comparison of the cryo-electron micrographs of a vitreous *P. aeruginosa* bacterium high-pressure frozen with PBS and 150 mM ammonium formate. The electron diffraction pattern corresponds to the bacteria frozen with ammonium formate and this confirms that the sample is vitreous.

The SOP for the high pressure freezing of bacteria and biofilms has been created and published on the project website. A procedure has also been put in place to ship vitreous samples between the partners, which can perform cryo-measurements: DOH, NPL and UNOTT, which included the use of dry-shipping for a safe, yet cryo-effective transport retaining the required level of cooling. The effectiveness of the shipping was tested using *P. aeruginosa* biofilms.

4.3.2 *Development of TERS probes and SERS substrates*

The aim was to develop procedures for the fabrication of efficient tip-enhanced Raman spectroscopy (TERS) probes and surface-enhanced Raman spectroscopy (SERS) substrates which are apt for highly sensitive Raman measurements on bacteria and biofilms. The work presented in this section was developed by INRIM with the support of UNOTT for the standard microbiology and CMI for the plasmonic simulations.

4.3.2.1 *Tip-Enhanced Raman Spectroscopy*

The two most widespread scanning probe microscopy (SPM) modes are atomic force microscopy (AFM) and scanning tunnelling microscopy (STM), and they can both be employed for tip enhanced Raman spectroscopy (TERS). While STM can achieve the best spatial resolution of the two and STM-TERS probes are less expensive and time-consuming to produce, its main limitation, the need for a conductive substrate, makes it unsuited for measurements on bacteria. AFM-TERS active tips are usually obtained from the gold or silver coating of commercial AFM tips because a good mechanical response of the cantilever is needed: for this fabrication, a layer of noble metal is applied on a standard silicon-based probe until a nanostructured apex whose plasmon response is tuned with the Raman laser is formed. This tuning is dependent on the nanoparticle size (the apex curvature radius), which is mostly dictated by the deposition technique, the layer thickness and the initial probe geometry. Hence, the optimisation of the tips is essential to achieve TERS on bacteria and biofilms.

While TERS is quite a promising technique, the reproducibility of the probes and spectra and the comparability of the results between the different instruments and laboratories are still open issues in the growing TERS community. In order for this technology to be adopted in commercial settings such as industry or in routine research, these limitations have to be overcome. In recent years, efforts have been made to develop standard procedures and reference samples for TERS, but the accurate evaluation of the enhancement factor (EF), remains an open issue. The accurate evaluation of the EF will enable a comparable characterisation of different enhancing tips, which is the most important variable in this kind of apparatus.

Producing effective Raman-enhancing tips has been an evolving matter of scientific investigation for the past two decades, and nowadays many approaches are available, but it is usually not possible to compare measurements among setups and laboratories without undertaking heavy biases, especially when aiming to perform intensity comparisons. In addition, the choice of parameters in SPM is known to influence the outcome of TERS measurements. In fact, the determination of many SPM parameters has a degree of arbitrariness in achieving a stable feedback, and setting the same experimental values across different probes does not guarantee the same physical condition. This is also due to the variability of the probes, which is influenced by many parameters, even in the same probe batches, because of a degree of randomness at the nanoscale in the fabrication processes.

Because of this, a procedure for the standardisation of the EF and precise TERS measurements on isolated tips was conceived and applied in the optimisation procedure for gold-coated AFM-TERS tips, and its precision was tested and compared to the EF standard assessment practice. A novel reference substrate for the interlaboratory comparisons and measurement of the spatial resolution of TERS was also developed.

4.3.2.1.1 <u>Model test system</u>

TERS probes were tested by exploiting the properties of selected molecules to form self-assembled monolayers (SAMs) on gold. Different molecules have been employed in these measurements in order to demonstrate the flexibility of the technique. The results were then compared with regular TERS measurements on the same analyte, and proper calculations of the EF have been made for each configuration and molecule. Three SAM-forming molecules were utilised for these measurements to test the flexibility of the procedure and to explore new analytes for plasmon-enhanced Raman: thiophenol, the de-facto standard for TERS studies, 7-mercapto-4-methylcoumarin (MMC), an alternative, more easily storable and manoeuvrable thiol, safer for human health, and thiram (tetramethylthiuram disulfide), a widespread pesticide and fungicide whose trace detection has practical real-world applications. To allow the formation of SAMs on gold, solutions of these compounds were prepared in ethanol (thiophenol: 5 mM; MMC: 1 mM; thiram: 8 mM) and the gold-covered probes were soaked in the solutions for 18 hours, then rinsed with ethanol and dried with a nitrogen flux. Measurements were made within 72 hours after the SAM preparation to avoid its degradation over time.

4.3.2.1.2 *Test procedure for enhancement assessment of AFM-TERS tips and an optimised fabrication procedure*

A method for the standardisation of the EF measurement in TERS was developed, in which the concept of TERS is extended as singular SERS to achieve a measurement on single nanoparticles. A schematic of the suggested standardisation method in comparison with a standard measurement on the same analyte is shown in Figure 22.
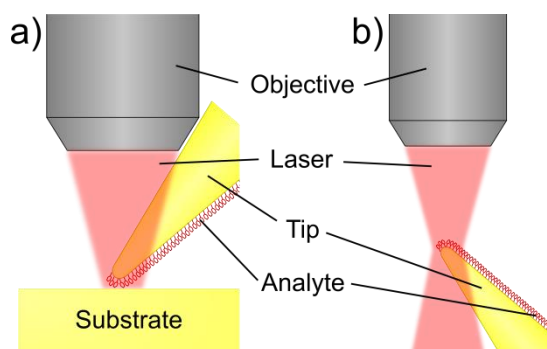

Figure 22. Gap-mode TERS measurement procedure for a target molecule (thiophenol) (a) compared to the proposed method with the isolated tip (b).

Thiophenol has been employed as a probe molecule in standardisation and interlaboratory comparison studies as a SAM chemisorbed on flat gold surfaces, measured in gap-mode TERS (as depicted in Figure 22a). This is a convenient and reproducible sample for both AFM- and STM-based TERS setups in any optical configuration, as it is conductive and mechanically stable, and it can be transparent for use with transmission microscopes.
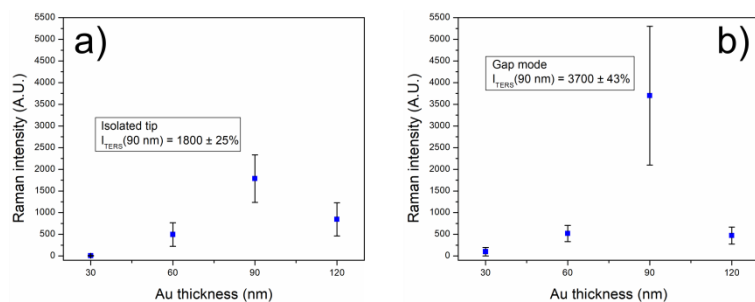

Figure 23. TERS intensities of thiophenol SAM chemisorbed on tip as a function of gold layer thickness on a silicon AFM probe with a 633 nm wavelength. (a): isolated tip mode; (b): gap mode. The same probes were used in both configurations.

The results of this study are presented in Figure 23, showing the means and standard deviations of TERS intensities from repeated measurements on different tips. As expected, both methods of measurement indicate the same optimal gold thickness of 90 nm, but gap mode generates more variable intense Raman signals of the analyte. The relative standard deviation of the intensities is 43 % on average for the measurements approached to a flat surface, while it is much less (25 %) for isolated TERS: this indicates that the proposed probe testing method actually decreases variability while achieving the same result. The mean EFs exhibited by thiophenol, MMC and thiram in gap mode and isolated tip configurations, with their respective uncertainties (based on statistics on repeated measurements with different tips), are reported in Table 2. The analysed Raman bands were the 998 cm^{-1} v_{CC} + δ_{CH} for thiophenol, the 1593 cm^{-1} v_{CC} of MMC, and the 1372 cm^{-1} δ_{CH3} from thiram.

Table 2. Estimated enhancement factors for each analyte.

Configuration	Thiophenol	MMC	Thiram
Isolated tip	$(4.6 \pm 1.6) \times 10^7$	$(2.3 \pm 0.6) \times 10^6$	$(2.3 \pm 0.7) \times 10^9$
Gap mode	$(1.0 \pm 0.5) \times 10^8$	$(6 \pm 3) \times 10^6$	$(4 \pm 2) \times 10^9$
Tip-tip dimer	$(3.0 \pm 1.0) \times 10^8$	$(1.7 \pm 0.5) \times 10^7$	$(1.4 \pm 0.4) \times 10^{10}$

4.3.2.1.3 *A new substrate for higher enhancement factors: tip-tip dimers*

To furtherly enhance Raman signals, an easily reproducible, large-area, conductive TERS substrate was conceived, consisting of a grid of mechanically stable, identical golden pyramids less than 1 μm in height protruding from a flat surface to be used as an array of sample tips in tip dimer experiments. A diagram of the fabrication procedure of the tipped substrate mentioned above is shown in Figure 24.
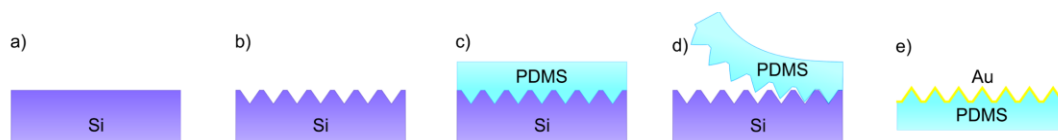

Figure 24. Imprinting lithography fabrication procedure for the tipped substrate employed for tip-tip dimers. A monocrystalline silicon wafer (a) is patterned and etched by a KOH solution until the surface has reverse pyramidal shaped holes (b); a 2 mm thick layer of liquid PDMS is poured on the surface (c), then baked until solid; the PDMS is then lifted off (d) and sputtered with 90 nm gold on a 5 nm titanium adhesion layer (e).

The sample was tested with the three SAM-forming analytes employed in the previous isolated tip study: each tip was covered in a SAM and employed isolated, in gap-mode and on a vertex of this tipped substrate in order to assess the enhancement capabilities with respect to the established techniques. The results of the EF calculations with formally calculated uncertainties are shown in Table 2. A comparison between nanoparticle configurations shows that gap mode yields EFs 2.2±0.4 times higher than the isolated nanoparticle geometry on average, and that the mean of the ratios between the EFs by the tip-tip dimers and the isolated tips is 6.7±0.6, demonstrating that tip-tip dimers are quite an effective enhancement method with respect to standard gap-mode.

4.3.2.1.4 *Test substrate for TERS spatial resolution*

A candidate sample suitable to achieve TERS chemical imaging traceability to the metre by means of an SPM based calibration procedure for nanometric accuracy was designed. It is designated to be both highly thermally and electrically conductive to minimise radiation heating and for measurements with both force-based and tunnelling current TERS feedbacks, making it a suitable candidate to be a universal TERS standard for calibration and comparisons, regardless of the apparatus specifications. Its gold surface, albeit flat, further enhances TERS signals, leading to measurements in gap-mode, resulting in much more intense signals than those arising from a non-gap mode TERS measurement and a much lower detection limit. The sample was manufactured as described in Figure 25.
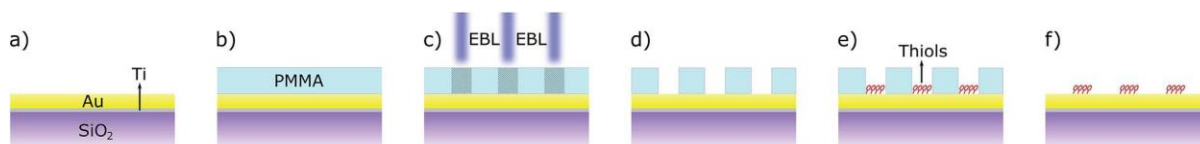
Figure 25. Scheme of the steps in the standard production process. The initial flat 20 nm Au surface (a), deposited on SiO₂ with a Ti adhesion layer, is covered by a 50 nm PMMA mask (b), which is then selectively exposed to EBL (c). After the mask development, bare Au areas remain (d), where thiols can selectively bond. The surface is soaked in a thiol solution until a self-assembled monolayer is formed (e), then rinsed, and sonicated in acetone to remove the mask. After this process, the gold surface with a nanopatterned thiol SAM is ready (f).

To test the sample, TERS chemical imaging in STM mode was performed with electrochemically etched silver tips on the finalised samples in order to verify the presence and the integrity of the monolayers, and that the masks were completely removed by the treatment. This was proven by the fact that no PMMA signal was measured on the surfaces. Moreover, it was verified that the portions of the surfaces that were supposed to remain pristine (because of the mask coverage and subsequent lift-off) were actually free of thiols, and that the molecules had not diffused onto them instead.
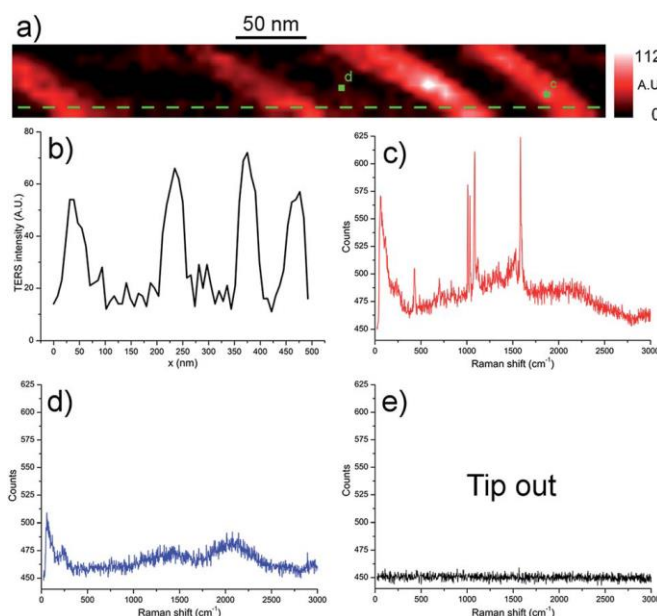

Figure 26. STM-TERS chemical map (a), without corrections, based on the 1074 cm-1 Raman peak, of a nanopatterned thiophenol surface, obtained with a 0.25 mW laser power and a 0.5 s per pixel integration time (pixel size 7.5 nm), and a line profile based on this signal (b), taken on the dashed line in (a). Raman spectra corresponding to the map are reported: a TERS spectrum on a SAM-covered area (c); a TERS spectrum corresponding to a bare gold pixel (d); a confocal Raman spectrum of the sample, measured with the tip retracted from the surface (e). The marks on the map indicate the pixels where the spectra (c) and (d) were taken.

In Figure 26, a TERS chemical map of one of the thiophenol-patterned surfaces is shown, the red colour represents the 1074 cm-1 peak intensity ($\nu CC + \delta CH$). Very defined parallel lines, corresponding to the spatial features previously measured on the PMMA masks, are clearly visible, and these are interspersed with zones with near zero intensity. An investigation of the corresponding spectra shows that no chemical was detected on these black areas, while pure benzenethiol spectra are registered on the lines corresponding to the organic pattern. In order to test the limits of the sample production process, a thinner pattern was drawn and a grating of thiophenol with lines roughly 8 nm wide were obtained. Lines with a width of (9 ± 4) nm were measured (the line width is defined here as the mean and standard deviation of the FWHMs of the Gaussian interpolations of several intensity profiles along the scans). Similar tests were performed with MMC as well, demonstrating the versatility of the concept of this sample.

4.3.2.2 Surface-Enhanced Raman Spectroscopy

A homogenous array of flexible gold-coated silicon nanowires (SiNWs) was fabricated by the combination of nanospheres lithography and metal assisted chemical etching (MACE) to obtain highly effective surface-enhanced Raman spectroscopy (SERS) substrates. A production method was developed, based on the combination of Nano Spheres Lithography (NSL), as a large-area surface patterning technique, and MACE, to achieve well-defined flexible gold-coated cylindrical SiNWs to support surface-enhanced Raman scattering. Our approach constitutes a low-cost alternative in the fabrication of ordered matrices of SiNWs, offering multiple degrees of freedom in the design and fabrication of SERS substrates, ranging from the micro to the nanoscale. Different 3D nanostructures can be constructed by adjusting parameters in order to change the inter-wire distance, the density of the wires on the surface as well as their length. The SERS efficiency of these substrates was investigated in different "leaning" and "non-leaning" wire configurations in order to select the

optimal configuration for Raman analysis. The work presented in the section below was developed by INRIM with the support of UNOTT for the standard microbiology and CMI for the plasmonic simulations.

4.3.2.2.1 *Model test system and measurements*

Melamine (Mel) was chosen as a probe molecule for the SiNWs thanks to their demonstrated properties to bind the gold surface, thus it is an ideal candidate to investigate the SERS mechanism occurring on the SiNWs based substrate (Mura, Martsinovich, & Kantorovich, 2008). Droplets of 100 µL Mel solution were deposited on leaning and non-leaning SiNWs samples and they were left to dry in air before Raman analysis. SAMs have been employed in the study of these SERS substrates as well. In particular, 7-mercapto-4-methylcoumarin (MMC) has been employed as a probe molecule in order to more accurately estimate the EF of the SERS substrates.

SERS measurements were taken with a commercial Thermo Scientific™ DXRxi™ Raman Imaging confocal microscope equipped with a 780 nm frequency-stabilised single mode diode laser as an excitation source, a 10x, 0.25 NA microscope objective, 50 µm slit and pinhole confocal apertures and an automatic motorised stage for mapping with a minimum horizontal step of 0.1 µm.

4.3.2.2.2 *Optimisation of the fabrication procedure of SERS substrates*

Silicon nanowires were fabricated by nanospheres lithography and metal-assisted chemical etching (MACE). A schematic of the process is shown in Figure 27. The adopted fabrication procedure gave a SiNWs matrix, which could be tested with SERS active molecules, the results of each step of the fabrication are shown in Figure 28. The ultimate substrates for SERS analysis consist of SiNWs with gold caps on top (Figure 28e) covering the diameter of the nanowires; the gold thickness was chosen to be 80 nm in order to ensure the maximum intensity in correspondence to a laser excitation wavelength of 785 nm.
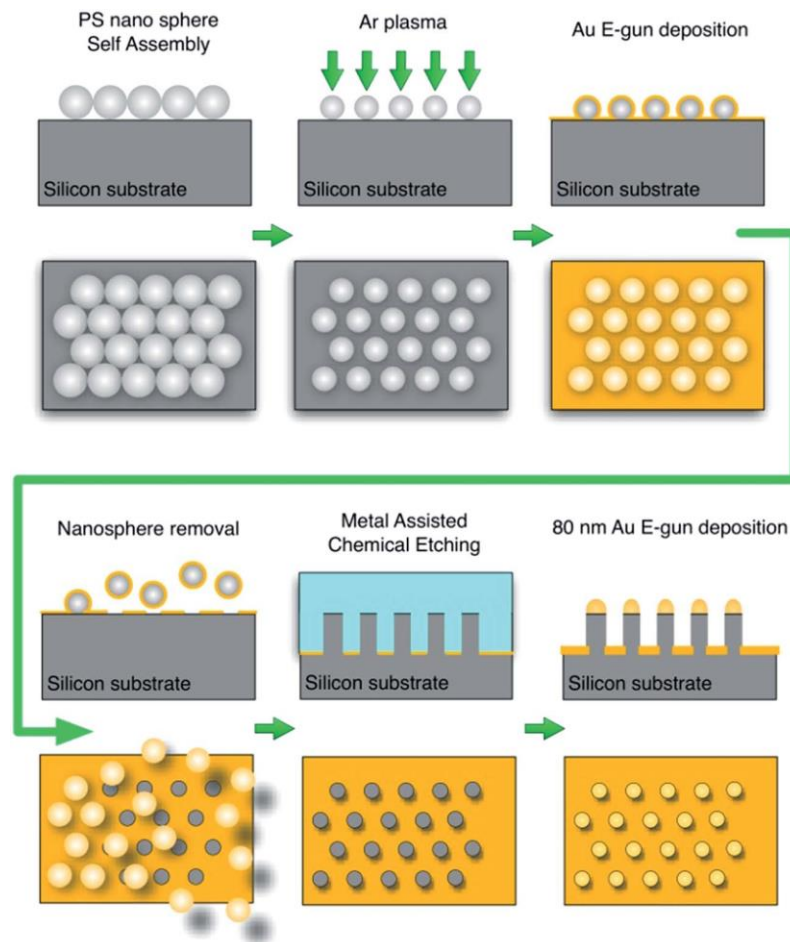
Figure 27. Schematic of the SiNWs SERS substrate production process.
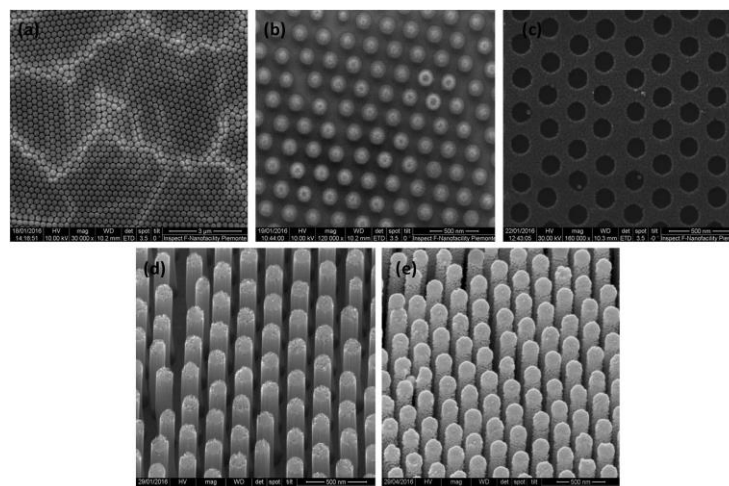
Figure 28. SEM images reporting consecutive steps of fabrication. (a) Monolayer of PS nanospheres self-ordered in hcp configuration in domains of some micrometres. (b) PS reduced nanospheres. (c) Au thin film patterned with circular voids resulting from the reduction of the nanospheres and their removal. (d) Resulting matrix of SiNWs. (e) SiNWs covered with 80 nm of gold.

The leaning of flexible nanostructures such as nanofingers or nanopillars coated with silver or gold is crucial for the intensity Raman enhancement. The flexibility of the free-standing silicon nanowires strongly depends on the length of the wires: leaning properties are impaired when this dimension is shorter than 0.6 mm. In order

to demonstrate that the SERS effect is magnified when flexible SiNWs are used due to the entrapment of the analyte in a multiple hotspots configuration, a SERS comparison test between leaning and non-leaning nanowires was performed (Figure 29). Moreover, the pre-leaned wires, i.e. wires brought to lean before the deposition of the analyte, and post leaning wires, wires brought to lean during the deposition of the analyte, were also compared to better understand the efficiency of the SERS mechanism.
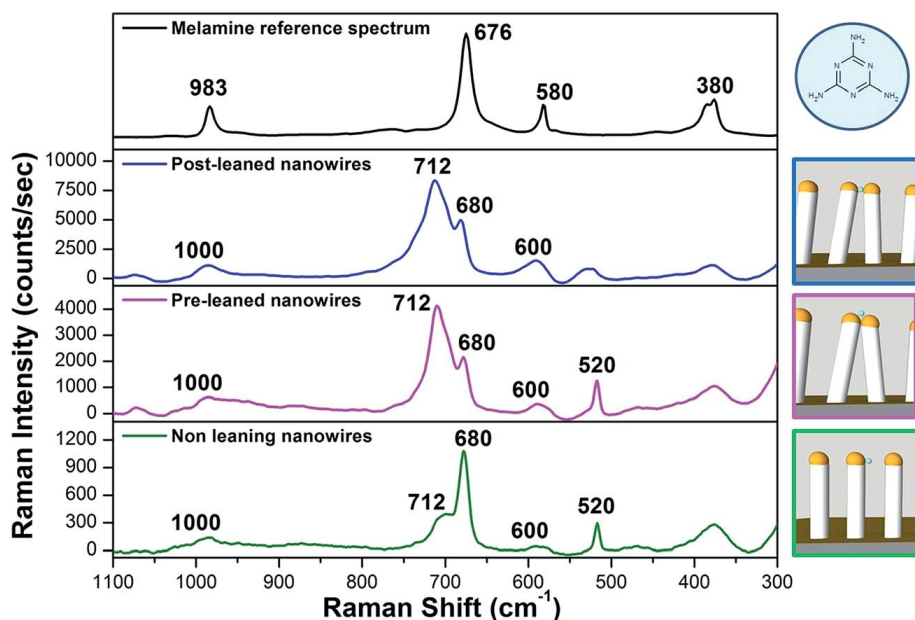

Figure 29. Reference Raman spectrum of melamine powder with the main assignments in the spectral region 300–1100 cm^{-1} (black line). Raman spectra recorded from post-leaned nanowires (blue line), pre-leaned nanowires (purple line) and non-leaning nanowires (green line) after the deposition of a 1 µL droplet of a 100 mg/L melamine solution on each substrate. Raman measurements were performed in air after the evaporation of the solvent.

SiNWs with an aspect ratio of 1:10 used in "post-leaned configuration" were selected as the optimized substrate (also considering that it provided a good homogeneity of the Raman signal across the droplet region), and the dynamic range of the substrate was investigated in order to obtain a calibration curve for quantification studies and to measure its sensitivity limit. Different concentrations of Mel solution ranging from 100 mg/L to 10^{-5} mg/L were deposited on the SiNWs substrates and they were characterised by Raman mapping. At least 50 spectra were collected and used for statistical analysis. An average relative standard deviation of 10 % of the Mel Raman signal at 712 cm^{-1} was calculated for each concentration value. A calibration curve was calculated in the range of concentrations between 10^{-8} mg/L to 10 mg/L by plotting the logarithm of the relative intensity ratio at 680 cm^{-1} over the intensity at 712 cm^{-1} with the logarithm of Mel concentration. A linear regression model was applied for the calibration and the forcefulness of the fit was confirmed by the reduced chi-square value which is attested close to 1 (Figure 30). The limit of detection (LOD) was experimentally detected on blank samples (n = 10) and calculated by the equation $LOD = M + 3s$ where M is the mean value of the relative intensity ratios at 680 cm^{-1} of the blank sample and s is the standard deviation. The limit of quantitation (LOQ) was estimated with the following equation $LOQ = 3.3\ LOD$. The LOD and LOQ were 3.20 x 10^{-7} mg/L and 1.00 x 10^{-6} mg/L, respectively. The present methodology is then suitable for melamine quantification in the concentration range of 1.00 x 10^{-6} mg/L to 10 mg/L. The EF of this SERS substrate was determined to be 1.3 x 10^{4}.
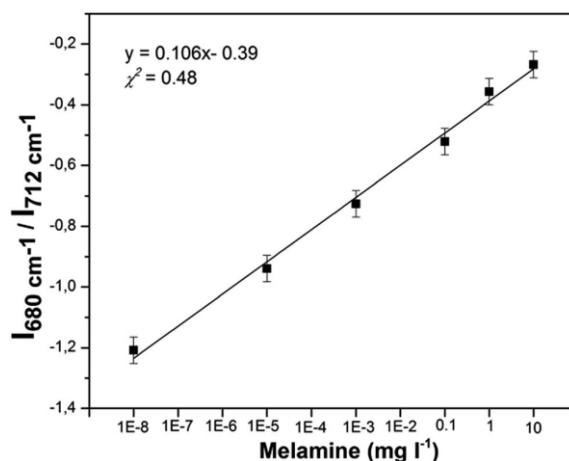
Figure 30. Calculated calibration curve.

The influence of the order of the SiNWs on SERS enhancement was also investigated, by investigating the variations in Raman signal of SAMs of MMC on substrates with varying degrees of order, a parameter quantified by measuring the correlation lengths (ξ) of surfaces prepared with different PS nanospheres (NSs) spin coating parameters. The self-assembly (SA) mechanism of nanospheres during spin coating is quite complex. The process is influenced by several factors, including the dispersion properties of the colloidal solution (i.e. weight fraction, solvent volatility and viscosity) as well as the dynamic conditions during spin coating. The dynamic conditions are given by the rotational speed (ω) and the acceleration (α) adopted during the spin coating process. The modification of these parameters has a direct impact on the evaporation rate of the solvent in which the NSs are dispersed, on the centrifugal forces and the surface tension among the nanoparticles and ultimately on the efficiency of the SA process. In order to understand the relationship between the rotational speed and ξ, a set of samples was prepared in which ω was varied between 1000 rpm and 3500 rpm. α was simultaneously varied to maintain the ramp time constant to 3.05 s. For all the samples at different ω, the SEM micrographs were analysed, as it is useful to evaluate the topographical distribution of NSs and to extract the values of ξ. By setting a spinning speed of 1000 rpm, the formation of double layers of nanospheres was observed, it is worth noticing that the hcp ordering of the second layer is often substituted by square close packing, in this case it is not possible to perform any further lithographic process, thus the deposition parameter will be discarded in the subsequent experiments. By increasing ω, the layer of NSs becomes more compact and the formation of a monolayer is reproduced in the range between $1250 \le \omega \le$ 2000 rpm. On the other hand, the formation of an unpacked layer in all of the samples processed at $\omega \ge$ 2500 rpm was observed, where large portions of the surface were not covered by the nanospheres. From a practical point of view, the speeds between 1250 rpm and 2000 rpm were adequate to perform a subsequent ordered pattern-transfer process.
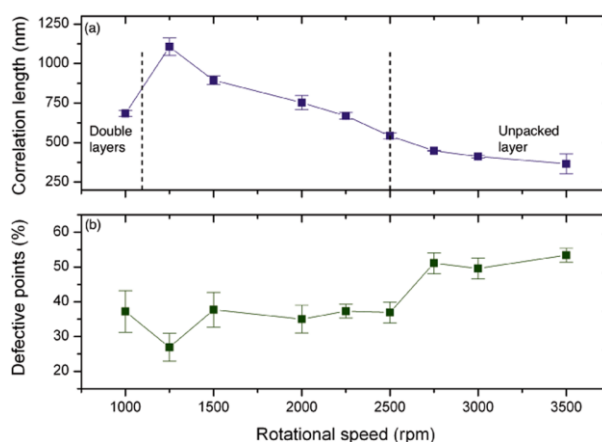

Figure 31. (a) The graph reports the monotonic decreasing trend of ξ at different rotational speed values. The maximum of ξ is found at 1250 rpm. (b) The graph shows the number of defects in the six-fold coordination of NSs in a monolayer on the substrate: the scatter plot refers to the sum of less and more of the six nearest neighbours to each particle.

Figure 31 summarises these measurements as ξ and the number of defective points as functions of ω. For values in the range 1250 ≤ω ≤3500 rpm, the obtained curve presents a monotonic decreasing trend with increasing spinning speed. For ω = 1250 rpm ξ reaches its maximum value, 1084 nm, and it drops to 339 nm for ω = 3500 rpm. The error bars are calculated as the standard deviation among ξ values extracted from different images for each substrate. The decrease of ξ to 1000 rpm can be associated to the presence of a second layer of NSs, as verified by electron microscopy micrographs.

Having determined the relationship between the deposition parameters and ξ, the influence of degree of order on the activity of the SERS substrate was inspected. For the purpose of this test, four samples with diverse values of ξ and in which the first step of deposition of the nanospheres was carried out by varying the spinning speeds were selected. These substrates will be referred to as NW1 (ξ = 1084 nm and ω = 1250 rpm), NW2 (ξ = 861 nm and ω = 1500 rpm), NW3 (ξ = 757 nm and ω = 2000 rpm) and NW4 (ξ = 339 nm and ω = 3500 rpm). The fabrication was completed by means of NSs reduction by plasma etching and MACE to obtain a two-dimensional array of gold-coated NWs; Figure 32 reports the fabrication steps and SEM images of the resulting substrates.
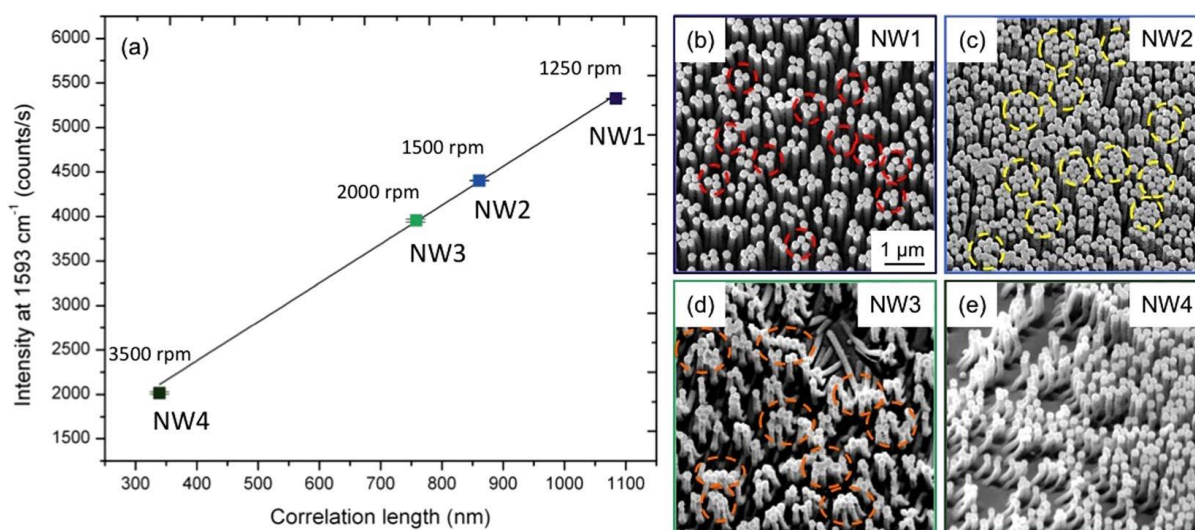

Figure 32. (a) Scatter plot of the average intensity of the SERS signal at 1593 cm⁻¹ from the four characterised substrates as a function of the correlation length ξ of the nanostructures. (b–e) SEM micrographs representing the disposition of the nanowires after the probe molecule deposition.

For this experiment, MMC was employed as the probe molecule. After the incubation of the SERS substrates with MMC and setting the most efficient configuration, corresponding to leaning nanowires, micro-Raman mapping was performed on the four chosen samples within an area of 0.5 mm^2 using a step size of 8 µm; the measurement was repeated eight times over each sample in a total area of 4 mm^2. The vibrational peak at 1593 cm⁻¹ was used to compare the enhancement given by different substrates. The values of the intensities of the characteristic peak for the four substrates are plotted against the correlation length ξ of the original monolayer of NSs in Figure 32. As evident from Figure 32a the ordered nanowires improve the enhancing capability of our substrates; the intensity is enhanced up to 5300 counts/s in the substrate NW1 with the largest correlation length and it progressively falls for decreasing order reaching below half of this value for substrate NW4. The error bars report the relative standard deviation of the eight repeated measurements. The presented trend can be motivated by the increase in the NWs density, and consequently the increase of the hotspot number in the most ordered substrate, coherently with the quality of the hcp configuration. However, the density alone is not enough to explain this result. The morphology of the hotspots has been investigated in the area with the largest enhancement by matching the SERS maps to the SEM analysis. The images in Figure 32b-e show the arrangement of the nanowires in the different substrates after the probe molecule's deposition. In agreement with (Ou, et al., 2011), the formation of bundles of two to five nanowires produces a greater enhancement of the electromagnetic field in proximity to the hot spot and this configuration is prevalent in the substrate NW1. The NWs bending configuration in substrates NW2 and NW3 was dominated by the formation of larger and irregular bundles leading to a lower enhancement of the SERS intensity. The bending

configuration of the NWs was strongly conditioned by the degree of order on the substrate. Thus, the correlation length can be identified as a substantial and easily measured parameter influencing both the density and the NWs bending arrangement playing a key role in the SERS signal enhancement. The EF was calculated for the most ordered and efficient substrate NW1, resulting in 1.6×10^6.

4.3.2.2.3 *Summary*

A procedure for the measurement of the TERS enhancement factor independently from the SPM apparatus, operator arbitrariness and most external factors was developed, in the form of an isolated tip covered in a SAM of organic molecules. This new standard procedure for the precise quantification of the EF allowed the optimisation of the AFM-TERS tips production process that is necessary for measurements on bacteria and biofilms. A novel substrate for further amplification of TERS signals was also engineered, consisting of a 2D array of pyramidal structures, showing promising results and high enhancements with respect to common techniques. Three target molecules were employed in these studies, from established standards to analytes with relevant real-life applications, and their results were compared while accurately measuring the EF of each molecule-configuration combination. The standardisation of TERS spatial measurement capabilities was also pursued, by means of a traceable spatial standard for TERS chemical imaging, which was conceived, constructed and tested with different organic compounds as target molecules. It was proven that this could be employed as a traceable universal standard for TERS spatial calibration.

For the production of SERS-active surfaces, a homogenous array of flexible, gold-coated SiNWs was obtained combining nanosphere lithography and metal assisted chemical etching. Melamine was used as an analyte probe molecule to test the performance of this SERS substrate in terms of the uniformity of the Raman signal across a large area, the sensitivity of the SERS substrate for analyte detection, and the analytical enhancement factor evaluation. The substrate demonstrated high uniformity, with a variability of the Raman response across the surface of only 10 %, and a high sensitivity; a calibration curve for melamine quantitative measurement was also constructed. In addition, the influence of the long-range ordering of the SiNWs distribution was studied as well, and the substrate was consequently optimised. The measurements showed a linear increase of the SERS signal for increasing values of correlation lengths, coherently with a more ordered and dense distribution of hotspots on the surface.

4.3.3 **Conclusions**

A series of generic signal enhancement strategies for a range of techniques has been developed, including cryopreservation methods, novel tips and substrates for Raman based techniques – TERS and SER. Some of the strategies have already been used for the analysis of bacterial samples across different project activities, such as the compatible with secondary ion mass spectrometry high pressure freezing of biofilms or the tips used for the s-SNOM analysis of triclosan-treated *E. coli.* The strategies can be further adopted by research and industrial communities to study, not only bacterial samples, but other biological systems. The third intended strategy for the nano sculpting of bacteria has been investigated but it has not brought the desired results. Several attempts have been made to produce bacterial lamellas especially for the s-SNOM analysis, but the measurements on these samples were unsuccessful. Future investigation is necessary.

5 Impact

This project has provided better, faster and more reliable tools for the scientific and industrial communities in sectors such as medical, pharmaceutical, medical devices and biomedical discovery.

A total of 11 papers have been published in peer-reviewed journals and are open access, and a further 3 papers have been submitted or are in preparation. Additionally, 42 conference presentations and posters were presented over the lifetime of the project. There were also a number of conferences, training sessions and workshops, where the results were shared with a variety of different stakeholders to aid the uptake of the work completed in this project. The dissemination included an interview on BBC World service 'The Inquiry' about antimicrobial resistance, seminars, communication with the public through "Massacre the microbes activity" at the University of Nottingham and a Schools study Day at Nottingham Castle.

Dissemination of the results will continue beyond the end of the project. There are several publications in preparation and also a number of talks and posters to be presented during upcoming meetings and conferences. In addition, there will be a stand showcasing bacteria and biofilm research, as a public

engagement, at The Royal Society summer exhibition in London in July 2019. Also, a special session, dedicated to MetVBadBugs will take place during the annual 18th ECASIA conference held in September 2019.

Impact on industrial and other user communities

This project advanced the measurement capability and provided the essential metrology needed for measuring drugs in bacteria and biofilms. This will have an impact across healthcare and industry sectors, including large pharma, clinicians, wound and infection centres and instrument vendors.

The implementation of the 3D OrbiSIMS instrument and the development of cryo-SIMS methodology will have an impact on research in all areas of drug discovery. It will enable researchers to perform high-resolution and high-sensitivity label-free 3D imaging of antibacterial agents in bacteria at the sub-cellular scale in their close to native state. This unprecedented measurement capability can be further translated to studies of animal and human samples and have impact on other life science sectors.

NPL has already started offering the 3D OrbiSIMS instrument as a measurement service. For example, a large pharmaceutical company has been using the methodology developed at NPL and expertise to study biofilms. The number of 3D OrbiSIMS instruments worldwide is increasing and this project contributed to the uptake of this technique and pioneered the essential metrology for the studies of bacterial samples.

The adaptation of the liquid cell has been assessed for the analysis of biological molecules and enabled the traceable quantification of the vertical concentration profiles of antibiotics in bacteria and biofilms. This will have an impact on a wide range of biological and biomedical research as it will enable studies of biological samples by XRF methods, which has not been possible thus far due to the high-vacuum requirements of these techniques.

The developed protocols for well-controlled bacterial model systems not only give insights into the mechanisms of antimicrobial resistance but also permit the same processes to be studied using different techniques, thus providing complementary information. Likewise, analysis instrument vendors will benefit from the availability of quantifiable reference samples for the benchmarking of methods and, in turn, advancing measurement capability.

The sensitivity of Raman techniques for complex biological samples have been vastly enhanced through the nanofabrication of nano-structured substrates (for SERS) and specialised tips (for TERS). These methods have been designed for studying bacterial samples but end users of the techniques are also expected to benefit as the developments could be translated and tailored to study other complex biological samples.

Impact on the metrology and scientific communities

The development of novel, beyond the state-of-the-art capabilities: cryo-3D OrbiSIMS, super-resolution 3D imaging, signal enhancement strategies for TERS and SERS measurements, quantitative XRF using a liquid cell and metrology for ambient-pressure and SI-traceable NAP-XPS have an important impact on the scientific communities. Good practice guides for well-controlled bacterial model systems and for cryogenic sample preparation have been produced and published, which are expected to have a significant impact to the wider community.

The consortium organised a successful focus meeting 'Cool tools for microbial imaging' at the Microbiology Society Annual Meeting 2018. The meeting highlighted that in recent years there have been extraordinary advances in the technologies available to study microbial biology. The development of new techniques to probe individual cells and molecules is a major driver of scientific advance. The focus meeting covered and showcased new advanced techniques that have been successfully applied to microbiology, including mass spectrometry imaging, light and electron microscopy and Raman spectroscopy. These have diverse applications which attracted a broad audience across all the Microbiology Society divisions.

Sample preparation is one of the most critical steps for reproducible high-resolution imaging. To ensure uptake of the results of this project and to promote the topic within the scientific community, NPL and NIBSC organised the 89th IUVSTA workshop "Biological and soft matter sample preparation for high-resolution imaging by high-vacuum techniques". The workshop attracted 58 people across a mixed audience (industry, academia etc.) for an extended scientific debate.

The project had a strong role in training, including e-Learning and webinars and teaching. Training courses for PhD students on the formation of biofilms were organised and there were series of two-day SPM workshops to improve the scientific community's knowledge of Graphics card-based computing for an inverse problem solution. Training was also given to the consortium in bacterial culturing and in the preparation of biofilms for imaging.

Impact on relevant standards

A technical report entitled "Surface chemical analysis of bacteria and biofilms" has been submitted to ISO TC 201 through DIN as a new work item proposal. The report summarises the current status of the characterisation of bacteria and biofilm by XPS, XRF, FTIR, IR-s-SNOM, SIMS, Raman-spectroscopy and super-resolution microscopy. This provides a good overview of the analytical techniques, requirements for sample preparation and what information each method provides in the context of biofilm analysis.

The adaptation of the liquid cell for a potential application to analyse biofilms using quantitative reference-free XRF was given as an outlook in the talk "Characterisation of bio-molecular nano-layers by means of reference-free X-ray Spectrometry".

A presentation was given at the annual workshop on AP-XPS in December 2017 about the development of instrumentation for measuring biofilms with NAP-XPS, and two application notes related to the subject were published.

The project's progress and engagement have been reported at all ISO TC 201, VAMAS and CCQM-SAWG and CCQM-CAWG meetings. The project enabled partners to provide input to the development of the existing and new standards. For example, contribution to a draft standard for the measurement of sputtering yield for organic materials and participation in a CCQM pilot study on 'the amount of substances at a buried interface'. Partners have been regularly involved in networking activities at user meetings and participated in standard- and technical committees especially: ISO TC 201, NA 062-08-16 AA and BIPM/CCQM SAWG.

Longer-term economic, social and environmental impacts

Economic benefits:

The O'Neill review on antimicrobial resistance (https://amr-review.org/) commissioned two independent studies by RAND Europe and KPMG, who modelled two scenarios for the situation in 2050. Using the available data, which under-reports AMR effects, they conservatively estimate that "300 million people are expected to die prematurely because of drug resistance over the next 35 years". The drop in the world's GDP will be between 2 % to 3.5 % with a corresponding loss of economic output between 60 and 100 trillion USD.

As an example, the Adult Intensive Care Unit (ICU) at the Queen's Medical Centre cares for >3500 critically ill patients every year. A single patient day in an intensive care unit costs the NHS more than £2 k, and mortality rates average approximately 20 %. The annual budget for Critical Care within just one hospital is more than £15 M. The potential benefit of interventions that reduce the length of stay and or clinical risk within this environment is huge.

The antibiotic resistance of bacteria, in the biofilm mode of growth, contributes to the chronicity of infections such as those associated with medical devices. Biofilms have become a common cause of medical, difficult-to-treat infections. The impact of the project could be seen from its potential benefits in treating chronic infections caused by biofilms. Chronic infections such as wounds cost the healthcare industry billions of dollars each year.

The results of the project are also expected to aid the pharmaceutical industry overall. With its annual output of € 220 B, its approximately 800,000 employees and as the world's major trader in medicinal products, the EU pharmaceutical industry is of strategic importance to the European economy. It is a major asset with regard to its contributions to economic growth, the labour market and the European science and technology base (estimated € 30,000 million in R&D in Europe in 2012). The world market for medical products is expected to reach nearly $1.17 trillion by 2017. It is therefore essential for the EU to maintain its competitive edge.

Social benefits:

The O'Neill review states that "Antimicrobial-resistant infections currently claim at least 50,000 lives each year across Europe and the US alone. As a result of AMR, modern health systems and treatments that rely heavily on antibiotics could be severely undermined". Surgery would become far more dangerous and too risky to

undertake. Modern chemotherapy drugs give increasingly successful patient outcomes but suppress the patient's immune system, making them susceptible to infections. In the last century, the world has witnessed a 50-fold decrease in maternal deaths and it is, more-or-less, taken for granted that childbirth is safe. Without action on AMR this modern-day concept will change.

Bacterial infection and biofilms are a major source of complications and even death upon severe surgical treatment and chemotherapy. Biofilms on implants are especially difficult to detect and treatment often fails due to the complex structure of the biofilm. This often requires the costly exchange of the implant and an impairment of life quality for years.

Environmental benefits:

The effects of antibiotics on the environment are still not entirely understood. However, one major concern is the rise of antibiotic-resistant strains of bacteria due to increased antibiotic use in humans and animals. This can critically disturb natural bacterial ecosystems and lead to a serious threat to human health. Biocidal Product Regulation (EU 528/2012) now requires evidence that a biocidal product will not give rise to microbial resistance. Increased research into new antibiotics and antibiotic alternatives is urgently needed to prevent the resistance from forming.

The developed technologies and methodologies are transferable to other biological systems or soft matter samples such as cells, tissues or food, and this will support uptake of the developed metrology by other academic and industry sectors, e.g. veterinary sciences, food production, marine biology, etc.

6   List of publications

1. T. Vignolini, L. Gardini, V. Curcio, M. Capitanio and F. S. Pavone, *Optimization of Highly Inclined Optical Sheet Illumination for Super-Resolution Microscopy*, Biophysical Journal 114 (3), 14a https://doi.org/10.1016/j.bpj.2017.11.121

2. Hornemann, D. Sinning, S. Cortes, L. Campino, P. Emmer, K. Kuhls, G. Ulm, M. Frohme, B. Beckhoff, *A pilot study on fingerprinting Leishmania species from the Old World using Fouriertransform infrared spectroscopy*, Analytical & Bioanalytical Chemistry 409 (29), 6907 – 6923 https://doi.org/10.1007/s00216-017-0655-5

3. P Sanjuan-Alberte, MR Alexander, RJM Hague, FJ Rawson, *Electrochemically stimulating developments in bioelectronic medicine,* Bioelectronic Medicine 4, 1 https://doi.org/10.1186/s42234-018-0001-z

4. SA Khaled, MR Alexander, DJ Irvine, RD Wildman, MJ Wallace, S Sharpe, *Extrusion 3D printing of unique geometries of paracetamol single formulation with tunable release profiles,* AAPS PharmSciTech 19 (8), 3403 – 3413 https://doi.org/10.1208/s12249-018-1107-z

5. J Meurs, MR Alexander, PA Levkin, S Widmaier, J Bunch, DA Barrett*, Improved extraction repeatability and spectral reproducibility for liquid extraction surface analysis–mass spectrometry using superhydrophobic–superhydrophilic patterning,* Analytical Chemistry 90 (10), 6001-6005 https://doi.org/10.1021/acs.analchem.8b00973

6. A Hüsler, S Haas, L Parry, M Romero, T Nisisako, P Williams*, Effect of surfactant on Pseudomonas aeruginosa colonization of polymer microparticles and flat films,* RSC Advances 8 (28), 15352-15357 https://doi.org/10.1039/C8RA01491D

7. M. Kjærvik, K. Schwibbert, P. Dietrich, A. Thissen, W.E.S. Unger*; Surface characterisation of Escherichia coli under various conditions by near-ambient pressure XPS*, Surface and Interface Analysis 50 (11), 996-1000 https://doi.org/10.1002/sia.6480

8. Eleonora Cara, Luisa Mandrile, Federico Ferrarese Lupi, Andrea Mario Giovannozzi, Masoud Dialameh, Chiara Portesi, Katia Sparnacci, Natascia De Leo, Andrea Mario Rossi & Luca Boarino*, Influence of the long-range ordering of gold-coated Si nanowires on SERS,* Scientific Reports 8, 11305 https://doi.org/10.1038/s41598-018-29641-x

9. Alessio Sacco, Dario Imbraguglio, Andrea M. Giovannozzi, Chiara Portesi and Andrea M. Rossia, *Development of a candidate reference sample for the characterization of tip-enhanced Raman spectroscopy spatial resolution*, RSC Advances 8 (49), 27863-27869 https://doi.org/10.1039/C8RA03762K

10. Hermann, P., Kästner, B., Hoehl, A., Kashcheyevs, V., Patoka, P., Ulrich, G., Feikes, J., Ries, M., Tydecks, T., Beckhoff, B., Rühl, E., and Ulm, G *Enhancing the sensitivity of nano-FTIR spectroscopy.* Opt. Express 25, 16574–16588. https://doi.org/10.1364/OE.25.016574

11. T Vignolini, L Gardini, M Capitanio, FS Pavone, *Quantitative imaging of efflux pumps in planktonic and biofilm-associated bacteria through single-molecule localization microscopy*, Proceedings of SPIE 11140 https://doi.org/10.1117/12.2535451

7 Contact details

None.

Works Cited

B. Beckhoff, B. K. (2006). Handbook of Practical X-Ray Fluorescence Analysis.

B. Beckhoff, e. a. (2009). A quarter-century of metrology using synchrotron radiation by PTB in Berlin. *Phys. status solidi*, vol. 246, no. 7, pp. 1415–1434.

Beckhoff, B. (2008). Reference-free X-ray spectrometry based on metrology using synchrotron radiation. *J. Anal. At. Spectrom.*, vol. 23, no. 6, p. 845.

Blum, C., Opilik, L., Atkin, J. M., Braun, K., Kammer, S. B., Kravtsov, V., . . . Zenobi, R. (2014). Tip-enhanced Raman spectroscopy - an interlaboratory reproducibility and comparison study. *Journal of Raman Spectroscopy, 45*, 22–31.

C. Streeck, T. W. (2018). Qualifying calibration samples for advanced thin film materials characterisation.

Cara, E., Mandrile, L., Lupi, F., Giovannozzi, A., Dialameh, M., Portesi, C., . . . Rossi, A. a. (2018). Influence of the long-range ordering of gold-coated Si nanowires on SERS. *Scientific reports*, 11305.

Chartier, C., Bastide, S., & Lévy-Clément, C. (2008). Metal-assisted chemical etching of silicon in HF–H2O2. *Electrochimica Acta, 53 (17)*, 5509-5516.

Clinical and Laboratory Standards Institute. (2012). Methods for Dilution Antimicrobial Susceptibility Tests for Bacteria That Grow Aerobically: Approved Standard-Ninth Edition M07-A9. pp. CLSI document M07-A9.

D. Grötzsch, C. S. (2017). A sealable ultrathin window sample cell for the study of liquids by means of soft Xray spectroscopy. *Review of Scientific Instruments* , 88, 123112.

F.V. Subach, e. a. (2009). Photoactivatable mCherry for high-resolution two-color fluorescence microscopy. *Nat. Methods*, doi:10.1038/nmeth.1298.

Fisher L. M., e. a. (1989). Ciprofloxacin and the fluoroquinolones. New concepts on the mechanism of action and resistance. *Am. J. Med.*, doi:10.1016/0002-9343(89)90010-7 .

Hess, S. T. (2006). Ultra-high resolution imaging by fluorescence photoactivation localization microscopy. *Biophys. J.* , 91, 4258–4272.

Kara, S., Keffous, A., Giovannozzi, A., Rossi, A., Cara, E., D'Ortenzi, L., . . . Gabouze, N. a. (2016). Fabrication of flexible silicon nanowires by self-assembled metal assisted chemical etching for surface enhanced Raman spectroscopy. RSC Advances.

Kloß S, e. a. (2013). Culture independent raman spectroscopic identification of urinary tract infection pathogens: A proof of principle study. *Anal. Chem.* , 85, 9610–9616 .

Love, J. C., Estroff, L. A., Kriebel, J. K., & Whitesides, R. G. (2005). Self-Assembled Monolayers of Thiolates on Metals as a Form of Nanotechnology. *Chemical Reviews, 105*, 1103–1170.

M. Kjaervik, K. S. (2018). Surface characterisation of Escherichia coli under various conditions by near-ambient pressure XPS. *Surf. Interface Anal.*

Mura, M., Martsinovich, N., & Kantorovich, L. (2008). Theoretical study of melamine superstructures and their interaction with the Au (111) surface. *Nanotechnology, 19*, 465704.

NCCLS. (2007). Performance Standards for Antimicrobial Susceptibility Testing. pp. doi:1-56238-525-5.

Ou, F., Hu, M., Naumov, I., Kim, A., W., W., Bratkovsky, A., . . . Li, Z. (2011). Hot-spot engineering in polygonal nanofinger assemblies for surface enhanced Raman spectroscopy. *Nano Letters, 11(6)*, 2538-2542.

Ovesný, M. K. (2014). STORM: A comprehensive ImageJ plug-in for PALM and STORM data analysis and super-resolution imaging. *Bioinformatics.*

P. Hermann, A. H. (2013). Near-field imaging and nano-Fourier-transform infrared spectroscopy using broadband synchrotron radiation. *Opt. Express*, 21, 2913–9.

S. Mastel, A. A. (2015). Nanoscale-resolved chemical identification of thin organic films using infrared near-field spectroscopy and standard Fourier transform infrared references. *Appl. Phys. Lett.*, 106, 023113.

Sacco, A., Imbraguglio, D., Giovannozzi, A., & Portesi, C. a. (2018). Development of a candidate reference sample for the characterization of tip-enhanced Raman spectroscopy spatial resolution. *RSC Advances*, 27863-27869.

Schröder, e. a. (2013). Combined dielectrophoresis-Raman setup for the classification of pathogens recovered from the urinary tract. *Anal. Chem.* , 85, 10717–10724.

Selvin, P. R. (2007). Fluorescence Imaging with One-Nanometer Accuracy (FIONA). *Cold Spring Harb. Protoc.* .

Stadler, J., & Zenobi, T. S. (2010). Nanoscale Chemical Imaging Using Top-Illumination Tip-Enhanced Raman Spectroscopy. *Nano Letters*, 4514-4520.

Tokunaga, M. I.-S. (2008). Highly inclined thin illumination enables clear single-molecule imaging in cells. *Nat. Methods* , 5, 159–161.

Vignolini, T. C. (2018). Characterization and improvement of highly inclined optical sheet microscopy. *Progress in Biomedical Optics and Imaging - Proceedings of SPIE* .

Vignolini, T. G. (2018). Optimization of Highly Inclined Optical Sheet Illumination for Super-Resolution Microscopy. *Biophysical Journal* , 114 (3), 14.

Whitesides, C. D. (1989). Formation of monolayers by the coadsorption of thiols on gold: variation in the length of the alkyl chain. *Journal of the American Chemical Society, 111*, 7164–7175.